

ORIGINAL RESEARCH ARTICLE

Rewiring of 3D Chromatin Topology Orchestrates Transcriptional Reprogramming and the Development of Human Dilated Cardiomyopathy

Yuliang Feng, MD, PhD*; Liuyang Cai, PhD*; Wanzi Hong, MD, PhD*; Chunxiang Zhang, MD, PhD*; Ning Tan, MD, PhD; Mingyang Wang¹, PhD; Cheng Wang, PhD; Feng Liu, PhD; Xiaohong Wang, MD; Jianyong Ma, MD, PhD; Chen Gao, PhD; Mohit Kumar², PhD; Yuanxi Mo, MD; Qingshan Geng, MD, PhD; Changjun Luo, MD, PhD; Yan Lin, BS; Haiyang Chen³, PhD; Shuang-Yin Wang, PhD; Michael J. Watson, BS; Anil G. Jegga, DVM, MRes; Roger A. Pedersen, PhD; Ji-dong Fu⁴, PhD; Zhao V. Wang⁵, PhD; Guo-Chang Fan⁶, PhD; Sakthivel Sadayappan⁷, PhD; Yigang Wang, MD, PhD; Siim Pauklin, PhD; Feng Huang⁸, MD, PhD; Wei Huang⁹, MD, PhD; Lei Jiang¹⁰, MD, PhD

BACKGROUND: Transcriptional reconfiguration is central to heart failure, the most common cause of which is dilated cardiomyopathy (DCM). The effect of 3-dimensional chromatin topology on transcriptional dysregulation and pathogenesis in human DCM remains elusive.

METHODS: We generated a compendium of 3-dimensional epigenome and transcriptome maps from 101 biobanked human DCM and nonfailing heart tissues through highly integrative chromatin immunoprecipitation (H3K27ac [acetylation of lysine 27 on histone H3]), in situ high-throughput chromosome conformation capture, chromatin immunoprecipitation sequencing, assay for transposase-accessible chromatin using sequencing, and RNA sequencing. We used human induced pluripotent stem cell-derived cardiomyocytes and mouse models to interrogate the key transcription factor implicated in 3-dimensional chromatin organization and transcriptional regulation in DCM pathogenesis.

RESULTS: We discovered that the active regulatory elements (H3K27ac peaks) and their connectome (H3K27ac loops) were extensively reprogrammed in DCM hearts and contributed to transcriptional dysregulation implicated in DCM development. For example, we identified that nontranscribing *NPPA-AS1* (natriuretic peptide A antisense RNA 1) promoter functions as an enhancer and physically interacts with the *NPPA* (natriuretic peptide A) and *NPPB* (natriuretic peptide B) promoters, leading to the cotranscription of *NPPA* and *NPPB* in DCM hearts. We revealed that DCM-enriched H3K27ac loops largely resided in conserved high-order chromatin architectures (compartments, topologically associating domains) and their anchors unexpectedly had equivalent chromatin accessibility. We discovered that the DCM-enriched H3K27ac loop anchors exhibited a strong enrichment for *HAND1* (heart and neural crest derivatives expressed 1), a key transcription factor involved in early cardiogenesis. In line with this, its protein expression was upregulated in human DCM and mouse failing hearts. To further validate whether *HAND1* is a causal driver for the reprogramming of enhancer-promoter connectome in DCM hearts, we performed comprehensive 3-dimensional epigenome mappings in human induced pluripotent stem cell-derived cardiomyocytes. We found that forced overexpression of *HAND1* in human induced pluripotent stem cell-derived cardiomyocytes induced a distinct gain of enhancer-promoter connectivity and correspondingly increased the expression of their connected genes implicated in DCM pathogenesis, thus recapitulating the transcriptional signature in human DCM

Correspondence to: Yuliang Feng, MD, PhD, Botnar Research Centre, Nuffield Department of Orthopaedics, Rheumatology and Musculoskeletal Sciences, University of Oxford Old Road, B4495, Headington, Oxford OX3 7LD, UK; or Siim Pauklin, PhD, Botnar Research Centre, Nuffield Department of Orthopaedics, Rheumatology and Musculoskeletal Sciences, University of Oxford Old Road, B4495, Headington, Oxford OX3 7LD, UK; or Feng Huang, MD, PhD, Institute of Cardiovascular Diseases, the First Affiliated Hospital of Guangxi Medical University, Nanning, Guangxi 530021, China; or Wei Huang, MD, PhD, Department of Pathology and Laboratory Medicine, University of Cincinnati College of Medicine, Cincinnati, OH 45267; or Lei Jiang, MD, PhD, Guangdong Provincial Geriatrics Institute, Guangdong Provincial People's Hospital, Guangdong Academy of Medical Sciences, Guangzhou, Guangdong 510080, China. Email yuliang.feng@ndorms.ox.ac.uk, siim.pauklin@ndorms.ox.ac.uk, huangfeng0813@gmail.com, huangwe@ucmail.uc.edu, or jianglei0731@gmail.com

*Y. Feng, L. Cai, W. Hong, and C. Zhang contributed equally.

This manuscript was sent to Yibin Wang, Guest Editor, for review by expert referees, editorial decision, and final disposition.

Supplemental Material is available at <https://www.ahajournals.org/doi/suppl/10.1161/CIRCULATIONAHA.121.055781>.

For Sources of Funding and Disclosures, see page 1681.

© 2022 American Heart Association, Inc.

Circulation is available at www.ahajournals.org/journal/circ

hearts. Electrophysiology analysis demonstrated that forced overexpression of *HAND1* in human induced pluripotent stem cell-derived cardiomyocytes induced abnormal calcium handling. Furthermore, cardiomyocyte-specific overexpression of *Hand1* in the mouse hearts resulted in dilated cardiac remodeling with impaired contractility/ Ca^{2+} handling in cardiomyocytes, increased ratio of heart weight/body weight, and compromised cardiac function, which were ascribed to recapitulation of transcriptional reprogramming in DCM.

CONCLUSIONS: This study provided novel chromatin topology insights into DCM pathogenesis and illustrated a model whereby a single transcription factor (HAND1) reprograms the genome-wide enhancer–promoter connectome to drive DCM pathogenesis.

Key Words: cardiomyopathy, dilated ■ chromatin ■ epigenomics

Clinical Perspective

What Is New?

- High-resolution 3-dimensional epigenomic mapping and comprehensive computational analyses were performed in human dilated cardiomyopathy (DCM) hearts.
- Enhancer–promoter connectomes are extensively rewired in human DCM and reside in preaccessible chromatin sites.
- HAND1 (heart and neural crest derivatives expressed 1) drives the rewiring of enhancer–promoter connectome to induce DCM pathogenesis.

What Are the Clinical Implications?

- DCM-enriched enhancer–promoter loops identified in this study could be developed as novel 3-dimensional genomic biomarkers for DCM.
- Targeting HAND1 might be used as a novel approach for therapeutic intervention for DCM.

Nonstandard Abbreviations and Acronyms

3D	3-dimensional
AAV9	adeno-associated virus 9
AIF1L	allograft inflammatory factor 1-like
cGMP-PKG	cyclic guanosine monophosphate–protein kinase G
ChIP-seq	chromatin immunoprecipitation sequencing
CRE	cis-regulatory element
DCM	dilated cardiomyopathy
E-P	enhancer–promoter
EGFP	enhanced green fluorescent protein
ENCODE	Encyclopedia of DNA Elements
EZH2	enhancer of zeste 2 polycomb repressive complex 2 subunit
Fbxo25	F-box only protein 25
FREM2	Fraser extracellular matrix complex subunit 1-related extracellular matrix 2

GAS1	growth arrest-specific 1
GFP	green fluorescent protein
GREAT	Genomic Regions Enrichment of Annotations Tool
H3K27ac	acetylation of lysine 27 on histone H3
HAND1	heart and neural crest derivatives expressed 1
HiChIP	highly integrative chromatin immunoprecipitation
hiPSC-CM	human induced pluripotent stem cell–derived cardiomyocyte
IGF-1	insulin-like growth factor 1
LRRC10	leucine-rich repeat containing 10
LRRC10B	leucine-rich repeat containing 10B
LV	left ventricular
MEF2D	myocyte enhancer factor 2d
MRPL20	mitochondrial ribosomal protein L20
MTSS1	MTSS I-BAR domain containing 1
MYH6	myosin heavy chain 6
MYH7	myosin heavy chain 7
MYPN	myopalladin
NFIB	nuclear factor I/B
NFIC	nuclear factor I/C
NPPA	natriuretic peptide A
NPPA-AS1	natriuretic peptide A antisense RNA 1
NPPB	natriuretic peptide B
PDE1C	phosphodiesterase 1c
PDLIM5	PDZ and LIM domain 5
RNA-seq	RNA sequencing
SLC16A2	solute carrier family 16 member 2
SMYD2	SET (suppressor of variegation, enhancer of zeste, trithorax) and MYND (myeloid-nervy-DEAF1) domain-containing protein 2
TAD	topologically associating domain
TBX5	t-box transcription factor 5
TGFβ	transforming growth factor–β
TUBA3D	tubulin alpha 3d
ZN563	zinc finger protein 563

Heat failure, the leading cause of death worldwide, affects >37.7 million individuals globally.¹ Dilated cardiomyopathy (DCM) is the most commonly diagnosed type of systolic heart failure.¹ No effective treatment can prevent the progression of DCM to heart failure. Heart transplantation, the last resort for patients with DCM, is hampered by limited donors and medical and economic burdens.² Thus, studies are urgently needed to demystify its pathogenesis and develop effective management strategies.

DCM is characterized by pathogenic structural remodeling of the left ventricle (ie, enlargement of the chamber and a thin ventricular wall) and poor contractility. Previous studies indicated that genetic variation in protein-coding genes (eg, sarcomeric and cytoskeletal genes) contributed to the pathogenesis of DCM in a minority of cases,³ suggesting that nongenetic (epigenetic) mechanisms may play a crucial role in DCM development.⁴ Because cell identity is primarily determined by coordinated gene transcription, novel insights into the mechanisms by which the DCM transcriptome is controlled will enable us to develop novel strategies to diagnose and treat DCM.

Gene transcription is regulated by a variety of determinants, and cis-regulatory elements (CREs), such as enhancers and promoters, are being recognized as the key determinants that shape gene expression.⁵ Dysregulation of CREs has been implicated in the pathogenesis of human diseases, such as thalassemia, polydactyly, and various types of cancers.⁶ During heart failure progression, the *MYH6/MYH7* (myosin heavy chain 6/myosin heavy chain 7) ratio is known to shift, as characterized by a decrease in *MYH6* expression and an increase in *MYH7* expression. A key enhancer has been identified to regulate the switch of *MYH6* expression to *MYH7* expression. Deletion of the predicted enhancer reduces *MYH7* and increases *MYH6* expression, leading to faster contraction in human engineered heart.⁷ To identify the potential CREs in human failing hearts, cap analysis of gene expression sequencing was performed in 3 healthy and 4 failed human left ventricles to map the initiation sites of both capped coding and noncoding RNAs.⁸ That study identified the transcribing promoters and the first intronic enhancer in failed ventricles but most distal enhancers (eg, intergenic enhancers) in heart failure were not explored. By performing chromatin immunoprecipitation sequencing (ChIP-seq) for H3K27ac (acetylation of lysine 27 on histone H3; an active enhancer and promoter mark⁹) in nonfailing and end-stage failing human heart tissues, a recent study identified specific enhancers and promoters implicated for established molecular pathways in heart failure.¹⁰ Nevertheless, the specific cis-regulome in DCM implicated for its pathogenesis remains unexplored.

Moreover, in many cases, enhancers regulate transcription through long-range interactions with target gene promoters, but not nearby gene promoters.¹¹

Thus, it is incorrect to assign the enhancer–promoter (E–P) pair only on the basis of the distance between the enhancer and promoter on the linear genome. Standard methods that map the E–P interactome at high resolution (kilobase) require a large number of cells/tissue samples and an extremely deep sequencing depth (billion reads per sample). New approaches to protein-mediated chromatin interactions (eg, highly integrative chromatin immunoprecipitation [HiChIP],^{12–14} proximity ligation-assisted chromatin immunoprecipitation sequencing,^{15,16} and in situ chromatin interaction analysis by paired-end tag sequencing¹⁷) have recently been developed to enable the generation of high-resolution chromatin contact maps for CREs with substantially reduced cell numbers and sequencing depth and can thus be applied to clinical samples, such as human DCM tissues, with high resolution.

Furthermore, the E–P interactome is embedded in topologically associated domains (TADs), which further aggregate into large-scale nuclear architectures called A/B compartments.¹⁸ In recent years, reorganization of higher-order chromatin architectures have been implicated in aberrant E–P interactions in human diseases (eg, abnormalities in limb development¹⁹ and gastrointestinal stromal tumors²⁰) and transcriptional derepression during cardiac lineage specification.²¹ However, the E–P interactome and its link to higher-order chromatin architectures in DCM remains unexplored.

In this study, we aimed to develop 3-dimensional (3D) epigenomic maps of DCM hearts and determine the main factors driving pathologic gene transcription in DCM. We leveraged these data sets to map the differential active CREs in DCM and nonfailing hearts, identify the differential active CRE interactomes and determine how the components are linked to transcriptional changes in DCM, investigate whether the formation of DCM-enriched CRE interactomes is related to higher-order chromatin structure (TADs and compartments) or chromatin accessibility, and uncover the key transcription factor that facilitates DCM-enriched CRE interactions and how it drives the pathogenesis of DCM.

METHODS

The data, analytic methods, and study materials will be made available to other researchers for purposes of reproducing the results or replicating the procedure. 3D epigenome mapping, bioinformatic analysis, human induced pluripotent stem cell-derived cardiomyocytes (hiPSC-CMs), mouse models, and all experimental approaches are detailed in the [Methods in the Supplemental Material](#).

Animal Studies

All research protocols conformed to the 2011 Guidelines for the Care and Use of Laboratory Animals published by the National Institutes of Health. All animal use protocols and experiments were performed according to the guidelines approved by the

Institutional Animal Care and Use Committee at Guangdong Provincial People's Hospital, South China University of Technology, and University of Cincinnati.

Human Studies

Acquisition of 101 human heart samples was approved by the institutional review board for the protection of human subjects at Duke University. De-identified frozen human heart samples with pathologic characterization were provided by the Duke Human Heart Repository, Department of Surgery at Duke University School of Medicine. In brief, left ventricular (LV) heart samples were collected from patients with DCM during surgery and the LV tissues were immediately dissected and snap frozen in liquid nitrogen. LV samples from nonfailing donor hearts served as controls. The heart sample characteristics are provided in [Table S1](#).

Statistical Analysis

Hypergeometric testing was used to detect significant chromatin interactions in HiChIP data. Negative binomial generalized log-linear model was used to model read counts in sequencing data and quasi-likelihood F test was used to identify differentially abundant features (eg, chromatin interactions, expressed genes, transcription factor binding peaks). Statistical analysis was performed with R version 3.5.1 or Prism 7.0 (GraphPad Inc). The statistical tests performed for each statistical graph are listed in the individual figure legends. For further details, see [Methods in the Supplemental Material](#).

RESULTS

Genome-Wide Identification of the Active CREs in DCM and Nonfailing Hearts

We used 50 human DCM and 51 nonfailing biobanked heart tissues ([Table S1](#)) to uncover novel mechanisms that regulate DCM pathogenesis by integrative analysis of multilayered 3D epigenomic features: transcriptome, epigenome, and 3D chromatin connectome. To accomplish this, we performed RNA sequencing (RNA-seq; $n=101$), ChIP-seq (H3K27ac; $n=20$), HiChIP (H3K27ac; $n=20$), in situ high-throughput chromosome conformation capture ($n=4$), and assay for transposase-accessible chromatin using sequencing ($n=20$) mapping ([Figure 1A](#)). Principal component analysis from RNA-seq data depicted a separation between DCM and nonfailing hearts, suggesting that the transcriptome of DCM is globally reconfigured compared with nonfailing hearts ([Figure S1A](#)). As CREs have been recognized as essential sequences for cell-specific transcription, we performed H3K27ac ChIP-seq^{9,22} on 10 DCM and 10 nonfailing human heart samples (left ventricle) to annotate active CREs. Principal component analysis showed a separation between the DCM and nonfailing samples ([Figure S1B](#)), indicating that the active CREs were differentially used in DCM and nonfailing hearts.

Because H3K27ac is associated with both promoters and distal enhancers,⁹ we then separated H3K27ac peaks

into promoter proximal peaks and enhancer peaks on the basis of their distances (± 2.5 kb) to known transcription start sites. Among the promoter regions, we identified 4446 DCM-enriched H3K27ac peaks (eg, promoters of the cardiac hypertrophy marker genes *NPPA* [natriuretic peptide A] and *NPPB* [natriuretic peptide B]²³), 1292 nonfailing-enriched H3K27ac peaks (eg, promoters of the normal cardiac marker gene *MYH6*²⁴ and the cytoskeleton marker gene *TUBA3D* [tubulin alpha 3d]²⁵), and 11 451 H3K27ac peaks common to both DCM and nonfailing hearts ([Figure 1B](#)). By integrating the RNA-seq data for those samples, we found that the expression of genes with DCM-enriched H3K27ac peaks on their promoters was significantly upregulated in DCM hearts compared with nonfailing hearts, whereas the expression of genes with nonfailing-enriched H3K27ac peaks was significantly downregulated, and the expression of genes with common H3K27ac peaks was unchanged ([Figure 1C](#)). We further corroborated these results by analyzing the expression of *NPPA*, *NPPB*, *MYH6*, and *TUBA3D* in human DCM and nonfailing heart tissues. *NPPA* and *NPPB* were significantly upregulated ([Figure 1D](#)), whereas *MYH6* and *TUBA3D* were significantly downregulated in DCM compared with nonfailing hearts ([Figure S1C](#)). These trends are consistent with the roles of H3K27ac in active transcription. The expression levels of *NPPA* and *NPPB* were highly correlated (Pearson correlation coefficient=0.751; [Figure S1D](#)), suggesting that they are coregulated at the transcriptional level and may share common regulatory elements.

Next, we identified 4204 DCM-enriched enhancers, 1626 nonfailing-enriched enhancers ([Figure 1E](#)), and 38018 common enhancers present in both DCM and nonfailing hearts ([Figure S1E](#)). By integrating 507 H3K27ac ChIP-seq data derived from different cells/tissues from the ENCODE project (Encyclopedia of DNA Elements), we further validated that the 4204 DCM-enriched enhancers displayed high cell specificity compared with 38018 common enhancers ([Figure 1F](#) and [Table S2](#)). In addition, we split the H3K27ac ChIP-seq data into cardiac ($n=18$) and noncardiac ($n=489$) cell types and found that H3K27ac peak regions in cardiac cell types overlapped significantly more DCM-enriched enhancers compared with noncardiac cell types ([Figure S1F](#)). These results suggested that DCM-enriched enhancers could play a role in orchestrating cell type-specific regulatory activity in DCM hearts. In line with this, GREAT (Genomic Regions Enrichment of Annotations Tool) analysis showed that DCM-enriched enhancers are located near genes essential for decreased muscle contractility, DCM, and abnormal myocardial fiber morphology ([Figure 1G](#)), suggesting the regulatory potential of these genes in DCM pathogenesis. DCM-enriched CREs can be exemplified by a genomic region on chromosome 1 ([Figure 1H](#)). This region contained a DCM-enriched enhancer near the coding gene *NPPB*. In addition, the

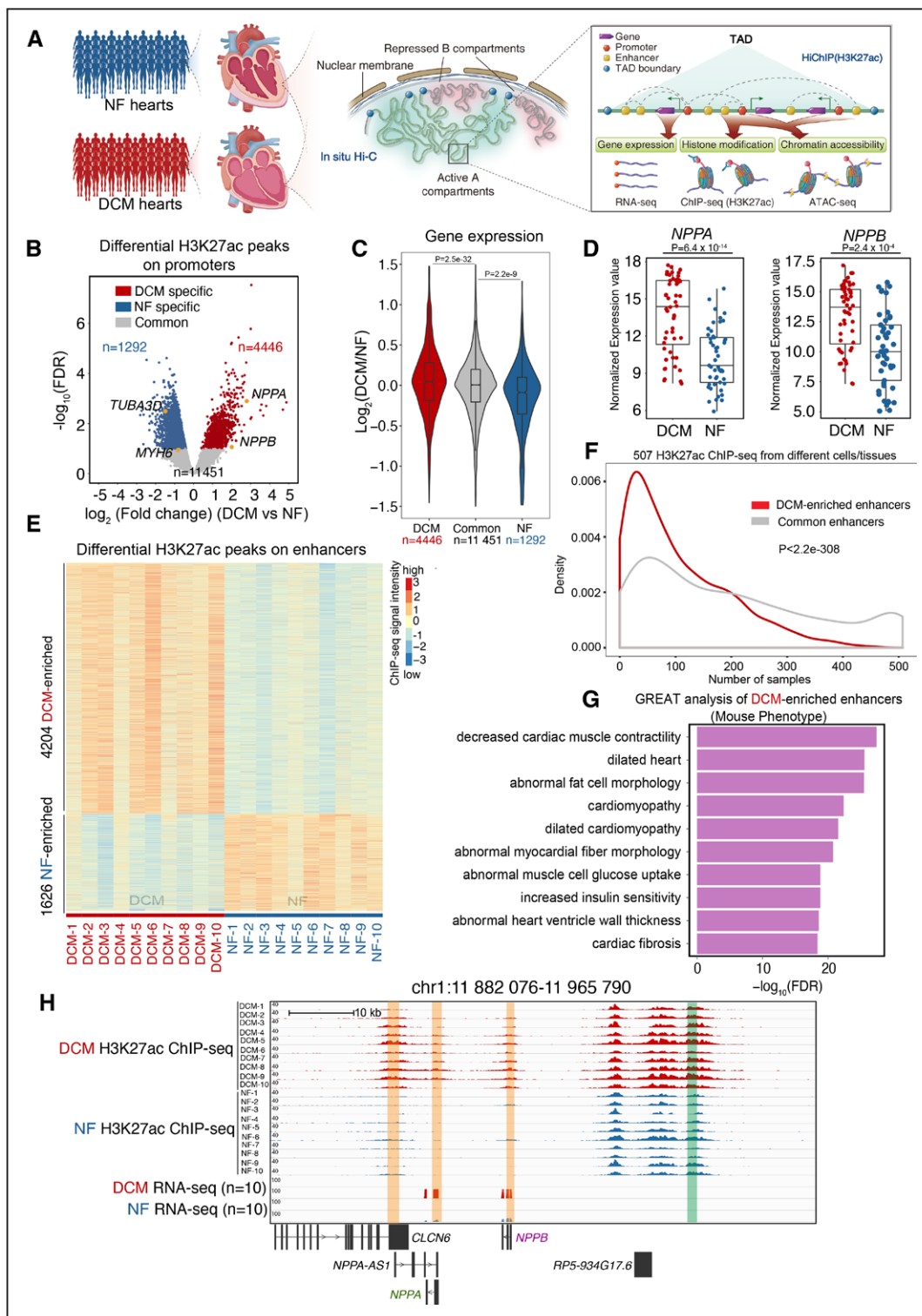


Figure 1. Genome-wide identification of active cis-regulatory elements in dilated cardiomyopathy and nonfailing hearts.

A. Schematic representation of 3-dimensional epigenome and transcriptome mapping for 50 dilated cardiomyopathy (DCM) and 51 nonfailing (NF) left ventricle heart tissue samples (left panel). In situ high-throughput chromosome conformation capture (Hi-C) was performed to examine the active A compartment and B compartment and topologically associating domains (TADs; middle panel). Highly integrative chromatin immunoprecipitation (HiChIP; H3K27ac [acetylation of lysine 27 on histone H3]) was performed to map the interactome of the active cis-regulatory elements (CREs), which was annotated by H3K27ac chromatin immunoprecipitation sequencing (ChIP-seq). Assay for transposase-accessible chromatin using sequencing (ATAC-seq) was used to identify chromatin accessibility on the CREs. (Continued)

Figure 1 Continued. RNA sequencing (RNA-seq) was used to measure transcription output (right panel). **B**, Volcano plot showing nonfailing-enriched ($n=1292$), DCM-enriched ($n=4446$), and common ($n=11451$) H3K27ac ChIP-seq peaks in promoter regions (within ± 2.5 kb of known transcription start sites) of DCM and nonfailing hearts. Cardiac hypertrophy marker genes (*NPPA* [natriuretic peptide A], *NPPB* [natriuretic peptide B]), normal cardiac marker gene (*MYH6* [myosin heavy chain 6]), and the cytoskeleton marker gene (*TUBA3D* [tubulin alpha 3d]) are labeled in yellow. **C**, Violin plot showing expression bias for genes exhibiting specific H3K27ac peaks in promoter regions (4446 DCM-enriched H3K27ac peaks, 1292 nonfailing heart-enriched H3K27ac peaks, and 11451 common H3K27ac peaks). Data were analyzed by Wilcoxon rank sum test with continuity correction. **D**, Expression values (\log_2 [normalized counts]) for *NPPA* and *NPPB* in 50 DCM and 51 nonfailing heart RNA-seq data sets. Data were analyzed by the Wald test. **E**, Heatmap of DCM-enriched ($n=4204$) and nonfailing-enriched ($n=1626$) H3K27ac ChIP-Seq peaks on enhancer regions in 10 DCM and 10 nonfailing heart samples (rows represent peaks and columns represent samples). **F**, Enhancer breadth (number of cells/tissues in which an enhancer is activated) of DCM-enriched and common enhancers. DCM-enriched enhancers (red) are significantly more represented as tissue-enriched than common enhancers (grey). Data were analyzed by Kolmogorov-Smirnov test. **G**, Bar chart showing the top 10 Gene Ontology terms (mouse phenotype from GREAT [Genomic Regions Enrichment of Annotations Tool] analysis) enriched for genes associated with DCM-enriched enhancers (ontology terms were ranked by negative \log_{10} [false discovery rate (FDR)] from smallest to largest). **H**, Genome browser view of *NPPA* and *NPPB* and their associated promoters and enhancers in DCM and nonfailing hearts. The enhancer is highlighted in the green box; the promoter is highlighted in the orange box.

NPPA-AS1 (natriuretic peptide A antisense RNA 1), *NPPA*, and *NPPB* promoters had specific H3K27ac peaks. A previous study demonstrated a cis-regulatory role for *NPPA-AS1* transcript in the repression of *NPPA* expression in atria.²⁶ However, *NPPA-AS1* was transcriptionally inactive, as shown from RNA-seq data, suggesting that this promoter may function in trans to regulate the transcription of other genes in DCM ventricle.

Taken together, the above results highlight that gene expression in DCM hearts is regulated by CREs and suggest that their interactions will bring to light the functions and target genes of these regulatory elements.

Characterization of the 3D Chromatin Organization in DCM and Nonfailing Hearts

The 3D connectome brings together regulatory chromatin regions and hence can potentially contribute to the regulation of gene expression. To map the high-resolution chromatin contact maps of active CREs, we performed H3K27ac HiChIP on 10 DCM and 10 nonfailing samples. We obtained ≈ 45 million high-quality paired-end reads (ie, unique valid interaction pairs) on average from the HiChIP libraries (Table S3). For the HiChIP data, we found that intergroup variation was greater than intragroup variation (Figure S2). HiChIP data contain both 1-dimensional (binding sites of the targeted proteins) and 3D (chromatin interactions between binding sites) information.^{12,13} We found that the 1-dimensional signals of the HiChIP data were comparable to those of the H3K27ac ChIP-seq data sets (Figure S3A). Inspection of the combined interaction matrix at different resolutions showed typical compartments (500-kb resolution), TADs (25-kb resolution), and focal loops (5-kb resolution) for both DCM and nonfailing hearts, similar to those reported in previous HiChIP data^{12,13} (Figure 2A). We then identified high-confidence chromatin interactions among gene promoters and distal enhancers in DCM and nonfailing hearts (Figure 2B). We found that 13562 promoters and 11308 enhancers were involved in chromatin interactions in DCM and that anchor genes had significantly higher expression than that of nonanchor

genes (Figure 2C), suggesting that chromatin interactions may play a role in transcriptional activation.

We then constructed chromatin interaction networks for DCM and nonfailing hearts separately, as genome-wide chromatin interactions are organized into giant modular interaction networks.²⁷ Promoters and enhancers were organized into chromatin interaction domains (Figure 2D) across the genomes of both DCM and nonfailing hearts; those interaction domains spanned similar genomic distances (Figure S3B) and contained most of the active promoters and enhancers (Figure S3C and S3D). The numbers of connected enhancers were positively correlated with increase in expression levels of their connected genes (Figure S3E). Chromatin interactions within the domains can first be classified as promoter-enhancer interactions (ie, gene promoters regulated by 1 or multiple enhancers). For example, the promoter of *PDLIM5* (PDZ and LIM domain 5), a gene involved in actin cytoskeleton organization in heart development²⁸ and DCM,²⁹ was regulated by an enhancer embedded in its intron (Figure 2E). Second, these chromatin interactions may be classified as promoter-promoter interactions. For example, both the *NPPA* and *NPPB* promoters have strong interactions with the *NPPA-AS1* promoter as shown by paired-end tags (Figure 2F), a finding that supports the conclusion that *NPPA* and *NPPB* may be coregulated by *NPPA-AS1* promoter. *NPPA-AS1* transcript is shown to have an inhibitory effect on *NPPA* expression in atria,²⁶ but our RNA-seq revealed that the *NPPA-AS1* gene is transcriptionally repressed in DCM ventricle. A recent study showed that nontranscribing promoters can have enhancer activity to regulate other gene transcription through chromatin looping,³⁰ in line with previous identification of enhancer-like promoters.^{31–33} To test whether *NPPA-AS1* promoter can function as an enhancer to regulate *NPPA* and *NPPB* expression, we performed luciferase reporter assays, a commonly used method for promoter and enhancer characterization³⁴ (Figure S3F). *NPPA* or *NPPB* promoter fragment was cloned upstream of the luciferase gene as the driving promoter and the *NPPA-AS1* promoter was cloned downstream of the luciferase gene as a presumed

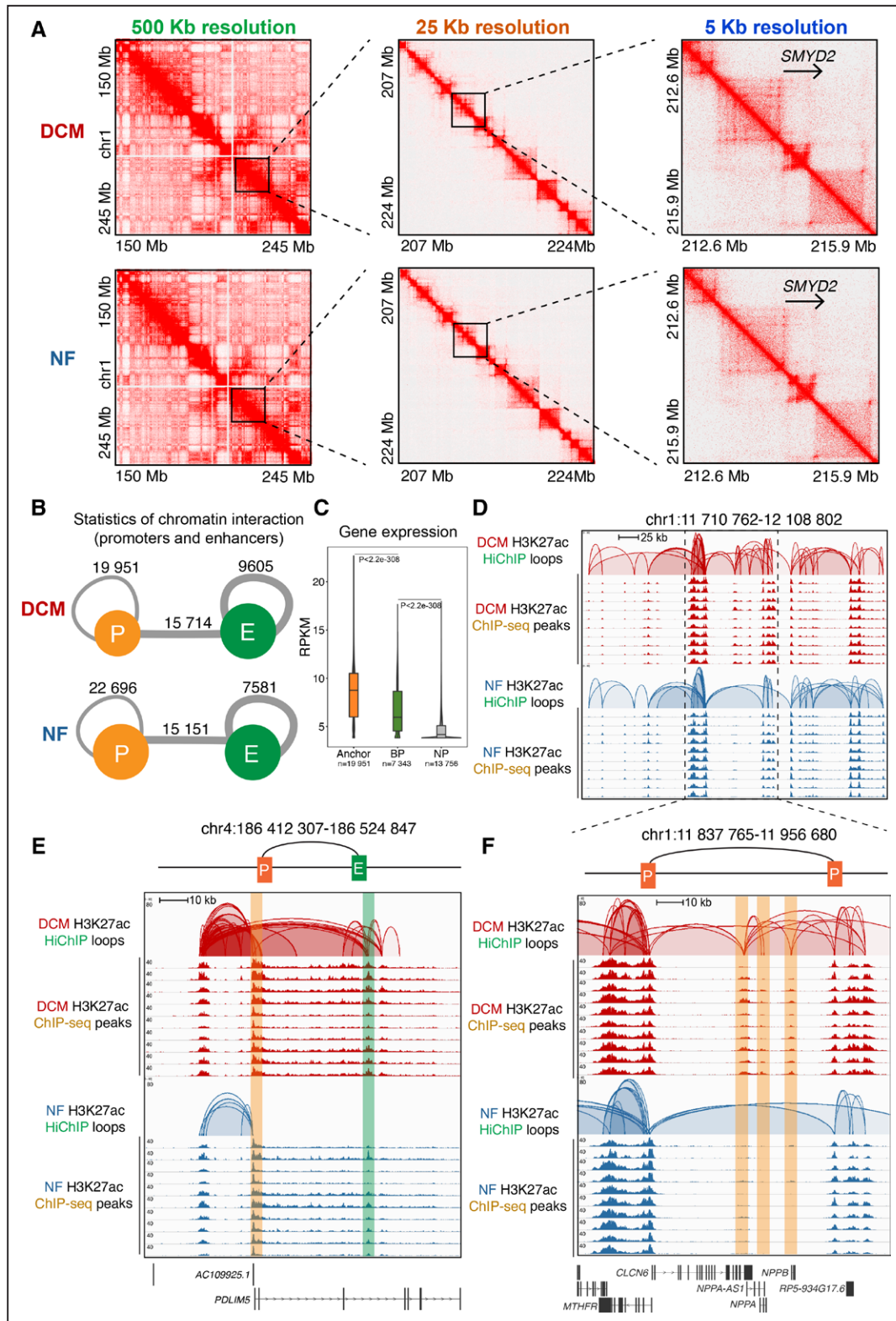


Figure 2. Characterization of the 3-dimensional chromatin organization of the active cis-regulatory elements by H3K27ac HiChIP in dilated cardiomyopathy and nonfailing hearts.

A, Knight-Ruiz matrix-balanced interaction maps of merged dilated cardiomyopathy (DCM; top) and nonfailing (NF; bottom) highly integrative chromatin immunoprecipitation (HiChIP) valid interaction pairs of typical compartments at 500 kb resolution (left), topologically associating domains (TADs) at 25 kb resolution (middle), and focal loops at 5 kb resolution (right). **B**, Summary of the number of chromatin interactions between promoters (P) and enhancers (E) in DCM (upper) and nonfailing (lower) hearts. **C**, Violin plot of expression levels for anchor genes ($n=19951$), basal promoter (BP) genes ($n=7343$), and nonpromoter (NP) genes ($n=13756$) in DCM. (Continued)

Figure 2 Continued. Data were analyzed by Wilcoxon rank sum test with continuity correction. **D**, Genome browser view of cis-regulatory element (CRE) interactions in chr1:11 710 762 to 12 108 802. The top 2 rows represent the CRE interactions in DCM hearts and the bottom 2 rows represent those in nonfailing hearts. The HiChIP loops and chromatin immunoprecipitation sequencing (ChIP-seq) peaks are shown for each. **E**, Genome browser view of enhancer–promoter interactions for *PDLIM5* (PDZ and LIM domain 5; chr4:186 412 307–186 524 847). The top 2 rows represent the interactions in DCM hearts and the bottom 2 rows represent those in nonfailing hearts. The HiChIP loops and ChIP-seq peaks are shown for each. The enhancer is highlighted in the green box; the promoter is highlighted in the orange box. **F**, Genome browser view of promoter–promoter interaction for *NPPA-AS-1* (natriuretic peptide A antisense RNA 1), *NPPA* (natriuretic peptide A), and *NPPB* (natriuretic peptide B). The top 2 rows represent the interactions in DCM hearts and the bottom 2 rows represent those in nonfailing hearts. The HiChIP loops and ChIP-seq peaks are shown for each. The enhancer is highlighted in the green box; the promoter is highlighted in the orange box. CLCN6 indicates chloride voltage-gated channel 6; H3K27ac, acetylation of lysine 27 on histone H3; MTHFR, methylenetetrahydrofolate reductase; RPKM, Reads per kilobase of transcript, per million mapped reads; and *SMYD2*, SET (suppressor of variegation, enhancer of zeste, trithorax) and MYND (myeloid-nervy-DEAF1) domain-containing protein 2.

enhancer, as enhancers generally function in a manner independent of orientation. The analysis of transfection and luciferase activity was performed in an in vitro cardiac hypertrophy model induced by endothelin-1 (10 nmol/L; 48 hours) in hiPSC-CMs. We found that the *NPPA-AS1* promoter alone was not able to activate luciferase gene expression. However, the *NPPA-AS1* promoter could act in concert with *NPPA/NPPB* promoter to significantly enhance the luciferase activity compared with *NPPA/NPPB* promoter alone (Figure S3G and S3H). This result indicated that the *NPPA-AS1* promoter could function as an enhancer to regulate *NPPA/NPPB* transcription. Overall, we identified the interactome of active CREs in DCM and nonfailing hearts in high resolution and uncovered that active promoters and enhancers were organized by multiple types of chromatin loops.

Specific E-P Connectome Regulates DCM-Specific Transcription

To examine how CRE interactions contribute to DCM-specific transcription, we performed differential analysis of HiChIP loops. Two classes of differential loops were identified on the basis of H3K27ac signal on loop anchors: class I (change of H3K27ac signal on loop anchors) and class II (no change of H3K27ac signal on loop anchors). For class I, we identified 670 DCM-enriched H3K27ac loops (DCM-enriched anchors) and 1035 nonfailing-enriched H3K27ac loops (nonfailing-enriched anchors; Figure 3A and Table S4). We found that these DCM-enriched H3K27ac loop-connected genes were significantly upregulated in DCM hearts (Figure 3B) and the nonfailing-enriched H3K27ac loop-connected genes were significantly downregulated in DCM hearts (Figure 3C). For class II, we identified 4883 DCM-enriched H3K27ac loops (common anchors) and 3712 nonfailing-enriched H3K27ac loops (common anchors; Figure S4A and Table S4). However, these differential loops have less interaction intensity (paired-end tag counts) compared with their counterparts in class I (Figure S4B) and their connected genes are not significantly linked to transcription change (Figure S4C and S4D). Hence, in downstream analysis, we focus on class I loops to explore the transcriptional regulation in DCM.

To understand the functional implications of the genes regulated by DCM/nonfailing-enriched H3K27ac loops, we represent their functional enrichment network³⁵ (Figure 3D and Figure S4E). For DCM-enriched H3K27ac loops, the most highly represented Gene Ontology terms included (1) molecular functions related to cytoskeletal protein binding and actin binding and (2) biological processes related to heart development, cardiac muscle development, adrenergic receptor signaling pathway, cardiac muscle hypertrophy, regulation of the force of heart contraction, response to insulin, muscle structure development, and striated muscle and differentiation. Pathway terms included cGMP-PKG (cyclic guanosine monophosphate–protein kinase G) signaling pathway, the IGF-1 (insulin-like growth factor 1) receptor, and longevity. Disease terms included, for example, cardiomyopathy (dilated), familial DCM, primary DCM, cardiomyopathy (familial idiopathic), and conduction disorder of the heart. These results suggested that specific E-P connectomes regulated specific transcription programs implicated in DCM development.

We uncovered specific examples of DCM-enriched E-P interactions. *TBX5* encodes a transcription factor crucial for proper cardiac development,³⁶ and we found that its promoter interacted with an activated enhancer embedded in its 7th intron in DCM hearts (Figure 3E). *SMYD2* (SET [suppressor of variegation, enhancer of zeste, trithorax] and MYND [myeloid-nervy-DEAF1] domain-containing protein 2; histone lysine methyltransferase) is robustly expressed in neonatal heart and regulates cardiac development and regeneration.^{37,38} Similar to *TBX5* (t-box transcription factor 5), we also found that its promoter interacted with an activated enhancer embedded in its 3rd intron in DCM hearts (Figure 3F). Other DCM-enriched E-P examples (*MEF2D* [myocyte enhancer factor 2d], regulator for myogenesis³⁹ and cardiac stress⁴⁰; *MYPN* [myopalladin], regulator for maintaining sarcomeric integrity⁴¹) are displayed in Figure S4F and S4G, respectively. These specific examples of DCM-enriched E-P interactions were validated by chromosome conformation capture quantitative polymerase chain reaction (Figure S4H). In addition to DCM-enriched E-P interactions, we also examined nonfailing-enriched E-P interactions. For example, *MRPL20* (mitochondrial ribosomal protein L20) encodes the large 39S subunit

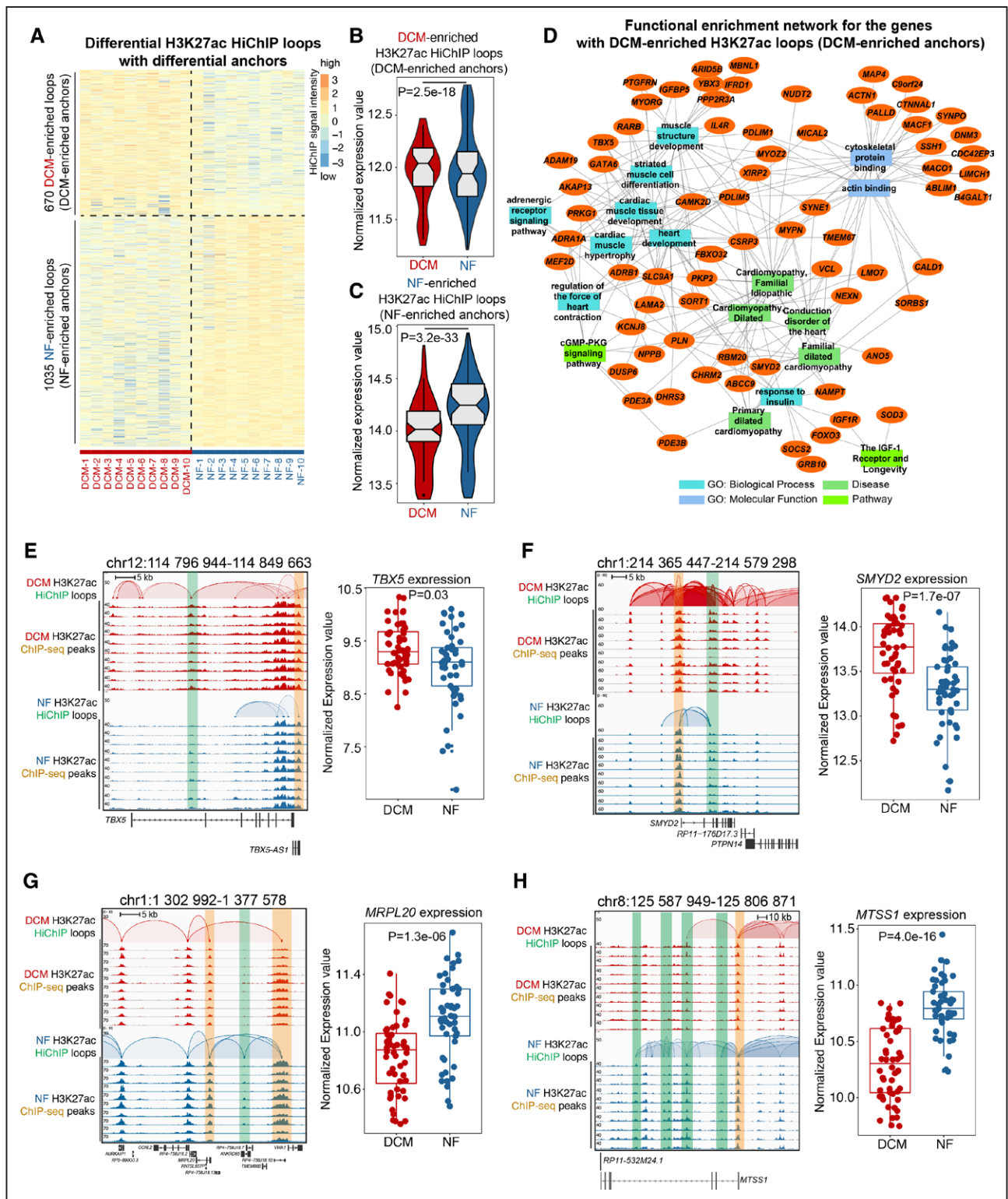


Figure 3. Dilated cardiomyopathy–enriched enhancer–promoter connectome contributes to dilated cardiomyopathy–specific transcription.

A, Heatmap showing the intensity of differential H3K27ac (acetylation of lysine 27 on histone H3) loops with differential loop anchors (H3K27ac signal) among 10 dilated cardiomyopathy (DCM) and 10 nonfailing (NF) heart samples. **B**, Normalized expression values of the genes with DCM-enriched H3K27ac loops (DCM-enriched anchors). Data were analyzed by Wilcoxon rank sum test with continuity correction. **C**, Normalized expression values of the genes with nonfailing-enriched H3K27ac loops (nonfailing-enriched anchors). Data were analyzed by Wilcoxon rank sum test with continuity correction. **D**, Network representation of functional enrichment of the genes with DCM-enriched H3K27ac loops (DCM-enriched anchors). Functional enrichment was performed using the ToppFun application. Orange nodes represent DCM-enriched genes; the different colored rectangles represent enriched terms. Only select enriched terms are shown here. (Continued)

Downloaded from <http://ahajournals.org> by on February 23, 2024

Figure 3 Continued. The network was generated using the Cytoscape application. **E**, Left panel: browser screenshot showing *TBX5* (t-box transcription factor 5) with DCM-enriched enhancer–promoter interactions (chr12:114796944–114849663). The top 2 rows represent the interactions in DCM hearts; the bottom 2 rows represent those in nonfailing hearts. The highly integrative chromatin immunoprecipitation (HiChIP) loops and chromatin immunoprecipitation sequencing (ChIP-seq) peaks are shown for each. The enhancer is highlighted in the green box; the promoter is highlighted in the orange box. Right panel: expression values (\log_2 [normalized counts]) for *TBX5* in 50 DCM and 51 nonfailing heart RNA-seq data sets. Data were analyzed by the Wald test. **F**, Left panel: browser screenshot showing *SMYD2* (SET [suppressor of variegation, enhancer of zeste, trithorax] and MYND [myeloid-nerve-DEAF1] domain-containing protein 2) with DCM-enriched enhancer–promoter interactions (chr1:214365447–214579298). The top 2 rows represent the interactions in DCM hearts and the bottom 2 rows represent those in nonfailing hearts. The HiChIP loops and ChIP-seq peaks are shown for each. The enhancer is highlighted in the green box; the promoter is highlighted in the orange box. Right panel: expression values (\log_2 [normalized counts]) for *SMYD2* in 50 DCM and 51 nonfailing heart RNA-seq data sets. Data were analyzed by the Wald test. **G**, Left panel: browser screenshot showing *MRPL20* (mitochondrial ribosomal protein L20) with nonfailing-enriched enhancer–promoter interactions (chr1:1302992–1377578). The top 2 rows represent the interactions in DCM hearts and the bottom 2 rows represent those in nonfailing hearts. The HiChIP loops and ChIP-seq peaks are shown for each. The enhancer is highlighted in the green box; the promoter is highlighted in the orange box. Right panel: expression values (\log_2 [normalized counts]) for *MRPL20* in 50 DCM and 51 nonfailing heart RNA-seq data sets. Data were analyzed by the Wald test. **H**, Left panel: browser screenshot showing *MTSS1* (MTSS I-BAR domain containing 1) with nonfailing-enriched enhancer–promoter interactions (chr8:125587949–125806871). The top 2 rows represent the interactions in DCM hearts and the bottom 2 rows represent those in nonfailing hearts. The HiChIP loops and ChIP-seq peaks are shown for each. The enhancer is highlighted in the green box; the promoter is highlighted in the orange box. Right panel: expression values (\log_2 [normalized counts]) for *MTSS1* in 50 DCM and 51 nonfailing heart RNA-seq data sets. Data were analyzed by the Wald test. cGMP-PKG indicates cyclic guanosine monophosphate–protein kinase G; GO, Gene Ontology; HiChIP, highly integrative chromatin immunoprecipitation; and IGF-1, insulin-like growth factor 1.

of mitochondrial ribosomes for protein synthesis within the mitochondria. We identified nonfailing-enriched E-P and promoter–promoter interactions for *MRPL20*, which are lost in DCM, suggesting its potential effect on mitochondrial dysfunction in DCM⁴² (Figure 3G). In addition, a recent study using integrated multiomics approaches such as RNA-seq and methylation assays identified *MTSS1* (MTSS I-BAR domain containing 1) as one of the key genes associated with LV systolic function.⁴³ We found that enhancer connectome associated with *MTSS1* promoter was lost in DCM as compared with nonfailing samples (Figure 3H), thus indicating its possible association with cardiac dysfunction in DCM. Other nonfailing-enriched E-P examples (*AIF1L* [allograft inflammatory factor 1-like], regulator for actomyosin contractility⁴⁴; *LRR10B* [leucine-rich repeat containing 10B], whose paralog *LRR10* [leucine-rich repeat containing 10] was ablated to induce DCM in mice⁴⁵) are displayed in Figure S4I and S4J, respectively. These findings indicate that DCM and nonfailing-enriched E-P interactions regulate genes involved in cardiac homeostasis.

DCM-Enriched E-P Connectome Largely Resides in Conserved Higher-Order Chromatin Architectures and Preaccessible Chromatin Sites Bound by Reactivated HAN1

Next, to investigate whether the altered H3K27ac looping in DCM is associated with changes in higher-order chromatin structures, we performed in situ high-throughput chromosome conformation capture on DCM and nonfailing heart tissue samples (left ventricles; Table S3 and Figure S5). In situ high-throughput chromosome conformation capture can capture the multilevel chromatin architecture, including the A and B compartments and TADs. We found that both the DCM and nonfailing heart genomes were partitioned into A and B compartments

(Figure 4A). We compared the A and B compartments in the genomes of nonfailing and DCM hearts; overall, only a small fraction (A to B, 13.3%; B to A, 9.4%) of the genome switched compartments from nonfailing to DCM hearts (Figure 4B). Gene expression was reduced for the genes that switched from the A to B compartment, whereas expression was increased for the genes that switched from the B to A compartment (Figure 4C); these results conform with previous findings showing that the A compartment corresponds to active transcription and that the B compartment corresponds to repressed transcription.¹⁸

Then we examined the TAD distribution and identified 1428 DCM-specific TADs, 1114 nonfailing-specific TADs, and 4803 common TADs (Figure 4D and Table S4). Comparison of genome-wide insulation scores suggested that TADs were highly conserved between DCM and nonfailing hearts (correlation coefficient, 0.97; Figure 4E) and presented similar insulation profiles (Figure 4F). Hence, the overall higher-order chromatin structures remain largely invariant from nonfailing to DCM hearts. Moreover, we found that the A and B compartments occupied similar portions of the genome, with TADs distributed evenly in the A and B compartments in both DCM and nonfailing hearts, whereas H3K27ac loops were located mostly in the A compartment, suggesting that H3K27ac-associated chromatin interactions are involved in active transcription (Figure S6A and S6B).

Furthermore, we aimed to determine the distributions of enriched H3K27ac loops in altered compartments and TADs in DCM and nonfailing hearts. We found that only 1.3% of DCM-enriched H3K27ac loops (Figure S6C) and 5.8% of nonfailing heart-enriched H3K27ac loops (Figure S6D) were in switched compartments. In addition, 9.4% of DCM-enriched H3K27ac loops (Figure S6E) and 15.5% of nonfailing-enriched H3K27ac loops (Figure S6F) were in changed TADs. The small percentage

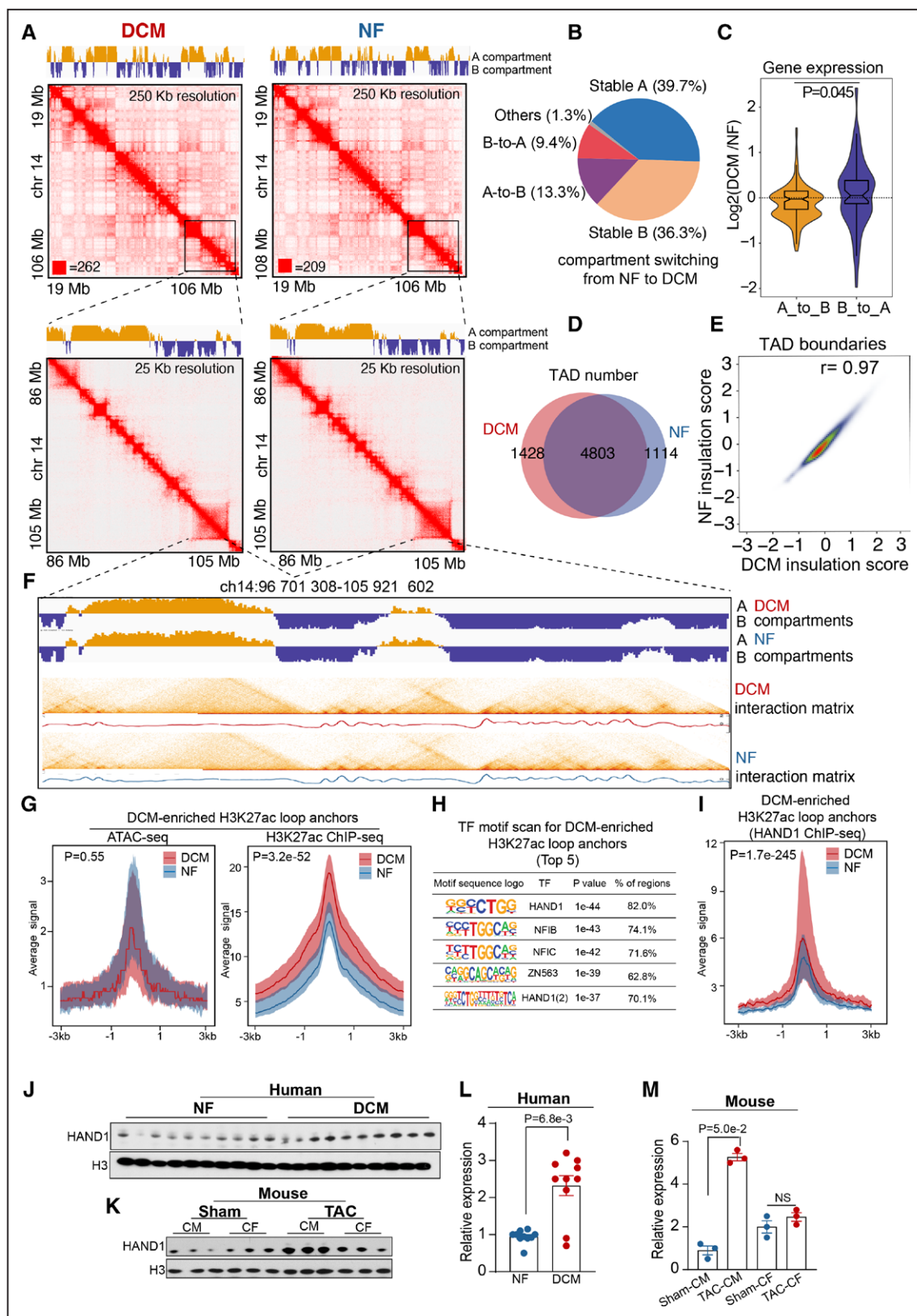


Figure 4. Dilated cardiomyopathy-enriched enhancer-promoter connectome largely resides in conserved higher-order chromatin architectures and preaccessible chromatin sites bound by reactivated HAND1.

A, Knight-Ruiz matrix-balanced interaction maps of merged dilated cardiomyopathy (DCM; left) and nonfailing (NF; right) in situ high-throughput chromosome conformation capture (Hi-C) valid pairs for DCM and nonfailing hearts at 250-kb and 25-kb resolution. The top tracks indicate the A (yellow) and B (blue) compartments. **B**, Proportion of genome switching between the A and B compartments (A to B [13.3%], B to A [9.4%], stable A [39.7%], and stable B [36.3%]) from nonfailing to DCM hearts. **C**, Expression bias in A to B and B to A compartment-switched (*Continued*)

Figure 4 Continued. genomes in DCM hearts normalized to expression in nonfailing hearts. Data were analyzed by Mann-Whitney *U* test. **D**, Venn diagram showing the number of topologically associating domains (TADs) in DCM hearts ($n=1428$) and nonfailing hearts ($n=1114$) and in both ($n=4803$). **E**, Correlation of insulation scores for DCM and nonfailing hearts; the Pearson correlation coefficient is indicated ($r=0.97$). **F**, A/B compartment, Hi-C contact map (heatmap), and corresponding insulation profiles for DCM and nonfailing hearts in the genomic region (ch14:96701308–105921602). **G**, Left panel: aggregation plot of DCM ($n=20$) and nonfailing ($n=20$) normalized assay for transposase-accessible chromatin using sequencing (ATAC-seq) signals ± 3 kb centered on the DCM-enriched H3K27ac (acetylation of lysine 27 on histone H3) loop anchors. Right panel: aggregation plot of DCM ($n=20$) and nonfailing ($n=20$) normalized H3K27ac chromatin immunoprecipitation sequencing (ChIP-seq) signals ± 3 kb centered on the DCM-enriched H3K27ac loop anchors. Data were analyzed by Mann-Whitney *U* test. **H**, Transcription factor motif scan for DCM-enriched loop anchors. The top 5 transcription factors are shown along with their motifs, *P* values, and percentage of regions. **I**, Aggregation plot of normalized HAND1 (heart and neural crest derivatives expressed 1) ChIP-seq signals ± 3 kb centered on the DCM-enriched H3K27ac loop anchors in DCM ($n=4$) and nonfailing ($n=4$) hearts. Data were analyzed by Mann-Whitney *U* test. **J**, Evaluation of HAND1 expression (normalized to H3 expression) in human nonfailing hearts and failing (DCM) hearts by Western blot analysis. **K**, Evaluation of HAND1 expression (normalized to H3 expression) in mouse cardiomyocytes (CMs) and cardiac fibroblasts (CFs) obtained from nonfailing hearts (sham) and failing hearts (8 weeks after transverse aortic constriction [TAC]) by Western blot analysis. **L**, Quantification of HAND1 expression in human nonfailing and DCM hearts. Data were analyzed by Mann-Whitney *U* test. **M**, Quantification of HAND1 expression in mouse cardiomyocytes and CFs isolated from sham and TAC hearts. Data were analyzed by Mann-Whitney *U* test.

of specific loops within altered compartments and TADs suggested that factors other than higher-order chromatin structures might underlie the formation of specific H3K27ac loops in DCM.

Because chromatin accessibility is essential for the function and interaction of CREs,⁵ we aimed to test whether DCM/nonfailing-enriched H3K27ac loop formation could be explained solely by chromatin accessibility. To this end, we developed an optimized assay for transposase-accessible chromatin using sequencing protocol⁴⁶ for frozen heart tissues (see [Methods in the Supplemental Material](#)) and performed the experiments on the same 20 DCM/nonfailing heart tissues described previously (Figure S6G). Compared with nonfailing hearts, DCM hearts had decreased chromatin accessibility for the nonfailing-enriched H3K27ac loop anchors (Figure S6H). However, chromatin accessibility was equivalent for the DCM-enriched H3K27ac loop anchors in DCM and nonfailing hearts (Figure 4G). These results suggested that DCM-enriched H3K27ac loops were formed on preaccessible chromatin regions.

Because transcription factors are key determinants shaping the 3D genome,⁴⁷ we scanned the transcription factor motifs on the DCM-enriched H3K27ac loop anchors that overlapped with their assay for transposase-accessible chromatin using sequencing peaks. The motifs for the transcription factors SMAD3⁴⁸ and MEF,⁴⁹ known to be involved in heart failure or DCM, were among the 20 most significantly enriched motifs (ranked 15 and 19, respectively; Figure S6I). The most significantly enriched transcription factor motif on the DCM-enriched H3K27ac loop anchors was HAND1 (heart and neural crest derivatives expressed 1; Figure 4H), which is not enriched in nonfailing-enriched H3K27ac loop anchors (Figure S6J). HAND1 is a basic helix-loop-helix transcription factor that is highly expressed in the embryonic heart and essential for heart development and homeostasis. In humans and rodents, *HAND1* transcription in the adult heart is maintained at a much lower level than in the embryonic heart.⁵⁰ A recent report identified a heterozygous *HAND1* mutation in blood DNA from some Chinese familial patients with DCM.⁵¹ However, the func-

tional roles of HAND1 in 3D epigenome reprogramming and transcription regulation within DCM hearts remains unexplored.

To further uncover the link of HAND1 with DCM-enriched H3K27ac looping, we performed HAND1 ChIP-seq (Figure S6K). We found that HAND1 binding was preferably enriched on DCM-enriched H3K27ac loop anchors (Figure 4I) in DCM hearts compared with randomly permuted regions (Figure S6L), nonfailing-enriched H3K27ac loop anchors (Figure S6M), or nonfailing/DCM-all loop anchors (Figure S6N). Although we demonstrated no significant difference of *HAND1* RNA expression between human DCM and nonfailing hearts (Figure S6O), HAND1 protein expression in human DCM hearts was significantly upregulated compared with that in nonfailing hearts (Figure 4J and 4L), suggesting post-transcriptional/posttranslational modifications of HAND1 in DCM. To further analyze HAND1 protein expression in mouse failing hearts, we constructed a transverse aortic constriction model and isolated cardiomyocytes and cardiac fibroblasts at 8 weeks after transverse aortic constriction. We found that HAND1 protein expression was significantly upregulated in transverse aortic constriction cardiomyocytes but not in transverse aortic constriction cardiac fibroblasts as compared with sham controls (Figure 4K and 4M). These data suggest that HAND1 might be the potential transcription factor linked to the DCM-enriched CRE interactions in cardiomyocytes.

HAND1 Rewires E-P Connectome in Concordance With Transcriptional Changes Associated With DCM Pathogenesis in hiPSC-CMs

To examine the functionality of HAND1 in organizing E-P connectome of human cardiomyocytes, we transduced control and HAND1-overexpressing (*HAND1*^{OE}) adenovirus into hiPSC-CMs for 72 hours, which has emerged as a useful platform for disease modeling and therapeutic screening in DCM.⁵² We subsequently performed 3D epigenome mapping (H3K27ac HiChIP, H3K27ac ChIP-seq, HAND1 ChIP-seq, and RNA-seq; Figure 5A and

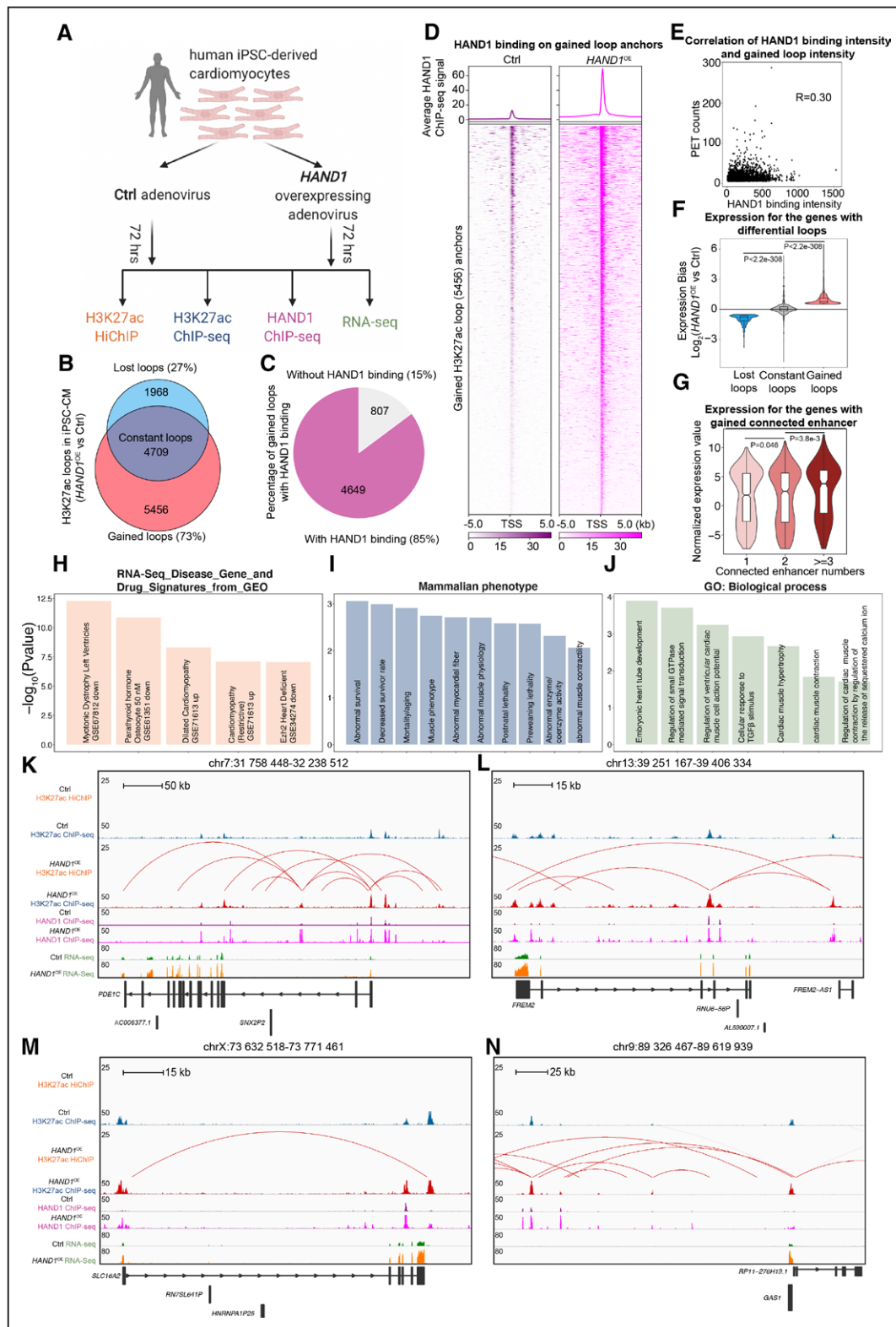


Figure 5. Overexpression of HAND1 rewires long-range enhancer–promoter connectome and transcriptome in human induced pluripotent stem cell–derived cardiomyocytes.

A, Schematic illustration of the experimental system and strategy to examine the roles of HAND1 (heart and neural crest derivatives expressed 1) in 3-dimensional chromatin organization and transcriptional control in human induced pluripotent stem cell (iPSC)–derived cardiomyocytes (hiPSC-CMs). **B**, Venn diagram showing the number of H3K27ac (acetylation of lysine 27 on histone H3) highly integrative chromatin immunoprecipitation (HiChIP) loops gained, lost, and constant in *HAND1*-overexpressing (*HAND1*^{OE}) vs control hiPSC-CMs. **C**, Percentage of gained H3K27ac HiChIP loops, the anchors of which do or do not overlap with HAND1 chromatin immunoprecipitation (*Continued*)

Figure 5 Continued. sequencing (ChIP-seq) peaks in *HAND1*^{OE} hiPSC-CMs. **D**, Aggregation plot and heatmap showing the intensity of *HAND1* ChIP-seq peaks on the gained H3K27ac HiChIP loop anchors (*HAND1*^{OE} vs control hiPSC-CMs). **E**, Correlation of the intensity of *HAND1* ChIP-seq peaks and the intensity of gained H3K27ac HiChIP loops in *HAND1*^{OE} hiPSC-CMs. **F**, Expression of genes with H3K27ac HiChIP loops gained, lost, and constant in *HAND1*^{OE} vs control hiPSC-CMs. Data were analyzed by Wilcoxon rank sum test with continuity correction. **G**, Normalized expression values for genes with gained H3K27ac HiChIP loops in *HAND1*^{OE} hiPSC-CMs, the promoter anchors of which connect with different numbers of enhancers. Data were analyzed by Wilcoxon rank sum test with continuity correction. **H**, Functional annotation (RNA-Seq_Disease_Gene_and_Drug_Signatures_from_GEO) for the genes with gained H3K27ac HiChIP loops. **I**, Functional annotation (mammalian phenotypes) for genes with gained H3K27ac HiChIP loops. **J**, Functional annotation (Gene Ontology [GO]; Biological Process) for genes with gained H3K27ac HiChIP loops. **K** through **N**, Examples of H3K27ac gained interactions (identified by H3K27ac HiChIP and ChIP-seq), *HAND1* binding (identified by *HAND1* ChIP-seq), and transcription (identified by RNA sequencing [RNA-seq]) in *HAND1*^{OE} vs control hiPSC-CMs. PET indicates paired-end tag; TGF β , transforming growth factor- β ; and TSS, transcription start site.

Figure S7A–S7C) in these cells. *HAND1* overexpression induced extensive rewiring of E–P connectome with more gained H3K27ac HiChIP loops ($n=5456$ [73%]) compared with lost loops ($n=1968$ [23%]; Figure 5B; global view of gained loops is demonstrated in Figure S7D). By integrating *HAND1* ChIP-seq data, we found that 85% of the gained loops were bound by *HAND1* on 1 or both anchors in *HAND1*^{OE} hiPSC-CM (Figure 5C). In addition, *HAND1* binding intensity is significantly higher in those gained loop anchors of *HAND1*^{OE} compared with control hiPSC-CM (Figure 5D). *HAND1* binding intensity is minimal on permuted regions (Figure S7E), but equivalent on common loop anchors (Figure S7F), and subtly less on lost loops (Figure S7G) in *HAND1*^{OE} compared with control hiPSC-CM, which further supported that gained loops are attributed to specific *HAND1* binding on the loop anchors. Moreover, *HAND1* binding intensity on the gained loop anchors is moderately correlated with loop intensity (Figure 5E). Taken together, these data indicate that the induced E–P rewiring is a direct effect of the upregulation of *HAND1*.

By integrating RNA-seq data, we found that genes within the gained and lost loops were significantly up- and downregulated, respectively (*HAND1*^{OE} compared with control hiPSC-CM; Figure 5F). In addition, in gained loops, the numbers of enhancers connected to promoters were significantly correlated with expression level (Figure 5G). Functional annotation analysis indicated that gained loops–associated genes overlapped with the transcriptional signatures in public human DCM RNA-seq data (Figure 5H). In line with this, we found that the genes (eg, *NPPA*, *NPPB*) upregulated in hiPSC-*HAND1*^{OE} (versus control) and DCM hearts (versus nonfailing) from this study are enriched in the transcriptional signatures of DCM and left ventricle hypertrophy (Figure S7H). Moreover, mammalian phenotypes for gained loops–associated genes showed significant enrichment in decreased survival, abnormal myocardial fiber, and abnormal muscle physiology/contractility (Figure 5I). Furthermore, Gene Ontology for gained loops–associated genes showed significant enrichment in biological processes associated with embryonic heart tube development, regulation of ventricular cardiac cell action potential, cardiac muscle hypertrophy, cardiac muscle contractility, and regulation of cardiac muscle contraction by regulating the release of sequestered calcium ion (Figure 5J), further validating

that some *HAND1* functions through activating chromatin looping and gene transcription involved in these processes during DCM pathogenesis. Examples of gained loops involving the well-established DCM driver gene *PDE1C* (phosphodiesterase 1c)⁵³ and unexplored genes *FREM2* (Fraser extracellular matrix complex subunit 1-related extracellular matrix 2), *SLC16A2* (solute carrier family 16 member 2), and *GAS1* (growth arrest-specific 1) are shown in Figure 5K through 5N. These results demonstrate that the upregulation of *HAND1* in hiPSC-CM results in the genome-wide gain of E–P contacts and concordant transcriptional activation of connected genes implicated in DCM development.

HAND1 Drives DCM Pathology in HiPSC-CM and Mouse Models

To test the pathologic effects of *HAND1* in DCM, we performed systematic in vitro and in vivo functional assays (Figure 6A). For in vitro study, we investigated the effect of *HAND1* overexpression on human cardiac morphology and function using adenoviral vectors to overexpress *HAND1* in hiPSC-CMs. At 72 hours after transduction, we found that a significantly higher percentage of *HAND1*-overexpressing hiPSC-CMs (hiPSC-CM^{*HAND1*}) were larger than null adenovirus transfected hiPSC-CMs (hiPSC-CM^{Null}; Figure S8A). Furthermore, overexpression of *HAND1* (hiPSC-CM^{*HAND1*}) resulted in significant increases in Ca²⁺ transient amplitude (Figure 6B), cell shortening, and relaxation velocity, respectively, compared with hiPSC-CM^{Null} (Figure S8B–S8D). These results indicated acute overexpression of *HAND1*-induced hiPSC-CM hypertrophy development with associated alteration in Ca²⁺ handling and contractility, which might be a compensation to maintain cardiomyocyte contraction.^{54–56}

To validate these results in vivo, we engineered an adeno-associated virus 9 (AAV9) vector with the *cTNT* promoter to drive cardiac-specific overexpression of *Hand1* in mouse cardiomyocytes (AAV9-*cTNT-Hand1*-EGFP [enhanced green fluorescent protein]; Figure 6C). To assess the specificity and potency of the *cTNT* promoter, AAV9 virus lacking *Hand1* (AAV9-*cTNT*-EGFP) was delivered to adult wild-type mice (8 weeks old; Figure S8E) at 3 different doses (5×10^{11} , 1×10^{12} , and 5×10^{12} viral genomes by intraperitoneal injection,

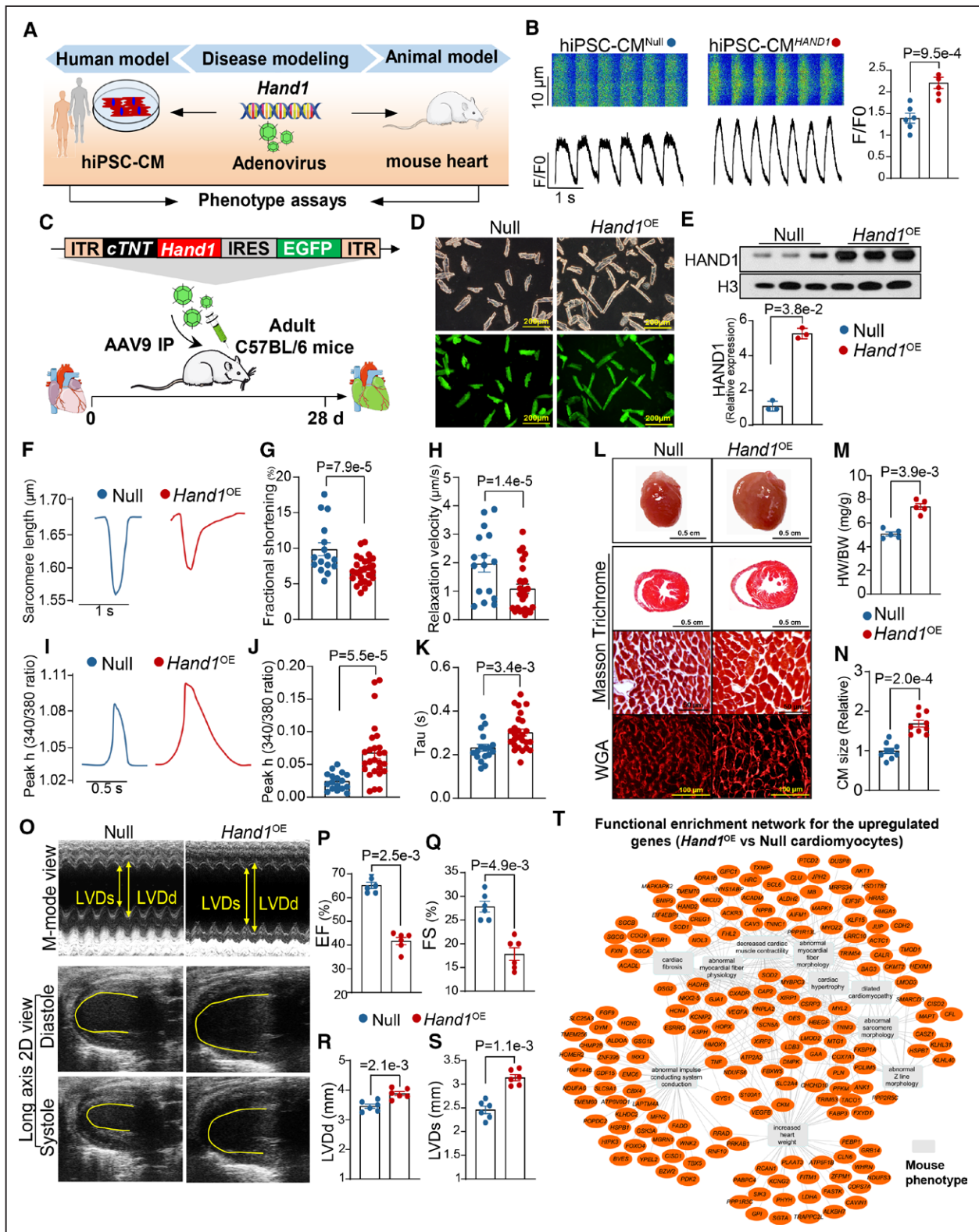


Figure 6. HAND1 induces dilated cardiomyopathy phenotypes in human induced pluripotent stem cell-derived cardiomyocytes and mouse hearts.

A, Experimental scheme for assessing *Hand1* (heart and neural crest derivatives expressed 1) pathogenicity in both human and mouse models with human induced pluripotent stem cell-derived cardiomyocytes (hiPSC-CMs) and mouse hearts, respectively. **B**, Representative calcium imaging recording traces and calcium transients to electric pacing at 1 Hz. hiPSC-CMs were transduced with adenoviruses carrying the cytomegalovirus promoter driving *HAND1* (hiPSC-CM^{HAND1}) or adenoviruses carrying only the cytomegalovirus promoter (hiPSC-CM^{Null}). Data were analyzed by the Student *t* test. **C**, Experimental scheme for evaluating adeno-associated virus 9 (Continued)

Figure 6 Continued. (AAV9)-driven *Hand1* overexpression in cardiac morphology and function. *Hand1* under the control of the *cTNT* promoter was cloned into an AAV9 backbone with an EGFP (enhanced green fluorescent protein) reporter (AAV9-*cTNT-Hand1*-EGFP). Animals were injected intraperitoneally and analyzed 28 days later. **D**, Representative images of cardiomyocytes isolated from AAV-treated hearts under light microscopy and fluorescence microscopy. The mice receiving injection of AAV9-*cTNT*-EGFP were designated as null and the mice receiving AAV9-*cTNT-Hand1*-EGFP injection were designated as *Hand1*^{OE}. **E**, Western blot assay for HAND1 protein expression in null and *Hand1*^{OE} hearts. Data were analyzed by Mann-Whitney *U* test. **F** through **H**, Contractility mechanic assay of mouse cardiomyocytes isolated from null and *Hand1*^{OE} hearts. **F**, Representative images of sarcomere shortening tracing. **G**, Cell shortening (%) at 0.5 Hz. **H**, Relaxation velocity of sarcomere at 0.5 Hz. Data were analyzed by Student *t* test. **I** through **K**, Ca²⁺ kinetics of mouse cardiomyocytes isolated from null and *Hand1*^{OE} hearts. **I**, Representative images of Ca²⁺ transient tracing. **J**, Ca²⁺ transient amplitude (peak h) as indicated by Fura-2 ratio (340/380 nm) at 0.5 Hz. **K**, Ca²⁺ decay time (τ) at 0.5 Hz. Data were analyzed by Student *t* test. **L**, Gross morphology (first row), Masson trichrome staining of gross morphology (second row), Masson trichrome staining of cardiomyocytes (third row), and wheat germ agglutinin (WGA) staining (bottom panel) of null and *Hand1*^{OE} hearts. **M** and **N**, Measurement of heart weight (HW) to body weight (BW) ratio (**M**) and cardiomyocyte size (**N**) in null and *Hand1*^{OE} mice. Data were analyzed by Mann-Whitney *U* test. **O** through **S**, Heart function was analyzed by echocardiography in null and *Hand1*^{OE} mice. **O**, Representative images of M-mode and long axis 2-dimensional views. **P** through **S**, Quantifications of left ventricular ejection fraction (EF; **P**), fractional shortening (FS; **Q**), left ventricular end-diastolic diameter (LVDd; **R**), and left ventricular end-systolic diameter (LVDs; **S**). Data were analyzed by Mann-Whitney *U* test. **T**, Network representation of functional enrichment of the upregulated genes in *Hand1*^{OE} cardiomyocytes (vs null). Functional enrichment was performed using the ToppFun application. Orange nodes represent dilated cardiomyopathy-enriched genes; gray rectangles represent enriched terms. The top 10 enriched terms are shown here. The network was generated using the Cytoscape application. *F*/*F*0 indicates peak amplitude relative to baseline fluorescence.

defined as low, medium, and high groups, respectively). The mice that received the same volume of saline were defined as the negative control group (designated as the saline group). Mice injected with the AAV9-*cTNT*-EGFP viral vector exhibited robust expression of GFP (green fluorescent protein) signal in cardiomyocytes (Figure S8F and S8G). As expected, no GFP signal was observed in saline-treated hearts. Although the AAV dosage was positively correlated with the number of GFP⁺ cardiomyocytes, no difference in the GFP protein level was observed between the medium and high groups (Figure S8F). These data indicate that 1 systemic dose of 1×10^{12} viral genomes yields highly efficient transduction in the majority of cardiomyocytes. We then used the selected dosage to intraperitoneally inject wild-type adult mice with AAV9-*cTNT-Hand1*-EGFP (designated as the *Hand1*^{OE} group) or AAV9-*cTNT*-EGFP (designated as the null group). AAV9 transduction in *Hand1*^{OE} hearts (Figure 6D) resulted in significant upregulation of HAND1, as determined by Western blotting (Figure 6E). To interrogate the functional effect of *Hand1* on heart failure progression, contractile mechanics, amplitude, and kinetics of intracellular Ca²⁺ transients were measured in freshly isolated mouse cardiomyocytes from *Hand1*^{OE} hearts and null hearts after AAV9 treatment for 4 weeks in vivo. In contrast to acute overexpression of *HAND1* in hiPSC-CMs, chronic overexpression of *Hand1* resulted in significant decreases in cell shortening and relaxation velocity, respectively, compared with the null cardiomyocytes (Figure 6F–6H). Although assessment of Ca²⁺ amplitude (peak h) revealed an increase in *Hand1*^{OE} cardiomyocytes, the τ was significantly prolonged compared with null cardiomyocytes (Figure 6I–6K), suggesting impaired Ca²⁺ handling. These results indicated the regulatory effect of *Hand1* on cardiomyocyte dysfunction progression, as evidenced by a decline in contractile function and abnormal Ca²⁺ handling.

Compared with the null hearts, the explanted *Hand1*^{OE} hearts were markedly enlarged (Figure 6L). In

addition, the heart to body weight ratios were higher in *Hand1*^{OE} mice than in null mice, indicating a significant increase in heart mass (Figure 6M). Using wheat germ agglutinin staining, we also found that the *Hand1*^{OE} cardiomyocytes were significantly larger than the null cardiomyocytes (Figure 6N), implying that cardiac hypertrophy was developed in the *Hand1*^{OE} cardiomyocytes. These effects were not the result of AAV9-induced toxicity as no changes in cardiomyocyte size were observed in mice transduced with AAV9 without *Hand1* (AAV9-*cTNT*-GFP) or in saline control mice (Figure S8H and S8I). Next, cardiac function analysis was examined in *Hand1*^{OE} mice and null mice by echocardiography (Figure 6O); compared with the null mice, the *Hand1*^{OE} mice showed significant reductions in LV ejection fraction and fractional shortening (Figure 6P and 6Q), which are key measures of cardiac contractile functions. Cardiac remodeling was also significantly increased in *Hand1*^{OE} mice, with increased LV end-diastolic diameter and LV end-systolic diameter (Figure 6R and 6S). To interrogate underlying mechanisms for HAND1-induced cardiac dysfunction, we performed RNA-seq in the cardiomyocytes isolated from null and *Hand1*^{OE} mice (Figure S8J). Differential analysis showed that HAND1 induced drastic transcriptome reprogramming in *Hand1*^{OE} cardiomyocytes (Figure S8K) and recapitulated the gene signatures in human DCM hearts (Figure S8L). Functional enrichment network analysis for the upregulated genes in *Hand1*^{OE} cardiomyocytes further showed that the most highly represented Gene Ontology terms included DCM, decreased cardiac muscle contractility, abnormal impulse conducting system conduction, cardiac hypertrophy, and increased heart weight (Figure 6T), which is in line with our observations in functional studies.

These data indicate that overexpression of *Hand1* in the adult heart provokes impaired contractility, Ca²⁺ mishandling, cardiomyocyte hypertrophy, and cardiac dilation and dysfunction. Taken together, our functional and

mechanistic data uncovered HAND1 as a novel factor in the development of DCM that could also serve as a therapeutic target for this heart disease.

DISCUSSION

Although 1-dimensional epigenome mapping techniques (eg, assay for transposase-accessible chromatin using sequencing and H3K27ac ChIP-seq) can identify CREs in the genome, they do not indicate the connectivity of CREs for transcription regulation. In contrast, high-resolution 3D genome techniques (eg, H3K27ac HiChIP) can identify the connectome of active CREs, which is

crucial because enhancers can skip their nearby promoters to regulate distal promoters.

In this study, we uncovered the 3D chromatin architecture in human DCM at high resolution and unraveled how this reorganization dictates transcriptional deregulation and its pathogenesis (Figure 7). We identified the DCM-enriched E-P connectome, which is largely dependent on preexisting chromatin accessibility and higher-order chromatin architecture, possibly priming their connected genes for rapid transcription in response to cardiac stress. We found that fetal cardiac and stress response genes (eg, *PDLIM5* [Figure 2E], *TBX5* [Figure 3E], *SMYD2* [Figure 3F], *MEF2D* [Figure S4F], *MYPN* [Figure S4G]) were

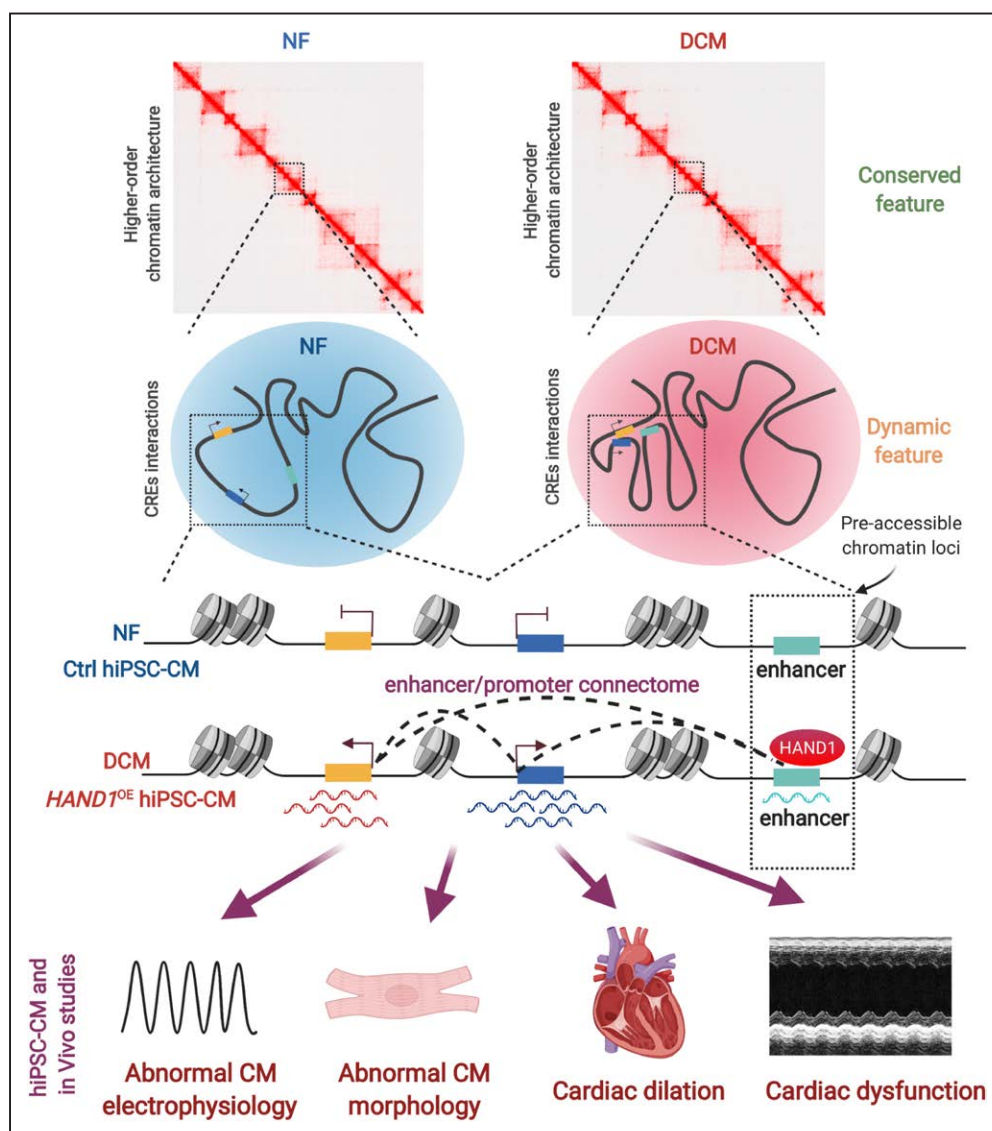


Figure 7. Model illustrating 3-dimensional epigenome organization in human dilated cardiomyopathy and how HAND1 rewires enhancer–promoter connectome to contribute to transcriptome reprogramming and dilated cardiomyopathy pathogenesis.

Dilated cardiomyopathy (DCM)–enriched enhancer–promoter connectome largely resides in preestablished, high-order chromatin architectures and preaccessible chromatin sites bound by reactivated HAND1 (heart and neural crest derivatives expressed 1). Ectopic expression of *HAND1* in human induced pluripotent stem cell–derived cardiomyocytes (hiPSC-CMs) and DCM hearts induces a distinct gain of enhancer–promoter connectivity and increases the expression of their associated genes implicated for DCM pathogenesis, leading to abnormal cardiomyocyte (CM) electrophysiology/morphology, cardiac dilation, and dysfunction. This illustrates a model whereby a single transcription factor rewires genome-wide enhancer–promoter connectome to drive DCM pathogenesis. CRE indicates cis-regulatory element; and NF, nonfailing.

aberrantly activated through gain of E-P loops, whose anchors are characterized by increased HAND1 binding. In line with this, overexpression of *Hand1* in adult mouse hearts also activated the expression of *PDLIM5*, *TBX5*, *SMYD2*, *MEF2D*, and *MYPN* (Figure S8L). This suggests that HAND1 may reactivate, at least in part, the early cardiac development and stress response genes in adult mice and humans to drive DCM pathogenesis.

HAND1 has not been investigated previously for a role in mediating long-range chromatin interactions. To test whether HAND1 could causally reprogram E-P connectome and transcription, we performed extensive 3D epigenome mapping in hiPSC-CMs. We found that HAND1 induces a genome-wide gain of distinct H3K27ac HiChIP loops. In addition, we showed that most of the gained loop anchors are characterized by increased HAND1 binding, indicating the direct effect of HAND1-induced chromatin looping. Moreover, the gained E-P connections increase the expression of their associated genes implicated for DCM, suggesting a direct functional connection with the disease. Furthermore, we showed that reactivation of HAND1 in hiPSC-CMs and mouse heart drives DCM phenotype and cardiac dysfunction, indicating that the precise temporal regulation of HAND1 is critical for cardiac homeostasis. Although 3D epigenome mapping indicates differential chromatin architectures in DCM compared with nonfailing hearts, these data sets have some limitations. These are bulk sequencing data that were obtained from hearts at the end stage of the disease at transplantation. As such, it is difficult to determine which of the many observed changes are disease casual, disease compensatory, or nonspecific changes that accompany any form of heart failure. Such insight is particularly challenging to obtain in humans because of ethical limitations. Nevertheless, the identification of HAND1 as transcription factor regulating the 3D chromatin connectomes, gene expression in DCM, as well as in mouse cardiomyocytes highlights the importance of this factor and its effects in playing an important causal role in this disease.

Although we identified the essential roles of HAND1 in chromatin looping, we also noticed that HAND1 binding is not always sufficient for loop formation and gene activation in induced pluripotent stem cell-derived cardiomyocytes, as some enhancers/promoters have strong HAND1 binding but are not involved in chromatin looping, suggesting that additional factors (eg, architectural proteins/transcription cofactors or chromatin-associated RNA) are required to facilitate HAND1-mediated E-P looping. Regarding this hypothesis, *in situ* capture of chromatin interactions by biotinylated dCas9 in induced pluripotent stem cell-derived cardiomyocytes, followed by proteomics and RNA-seq,⁵⁷ could identify HAND1-interacting proteins/RNAs involved in chromatin looping. In addition, how HAND1 and its associated factors work together to regulate 3D chromatin contact (eg, through phase-separated nuclear condensates⁵⁸) should be

addressed in the future. Moreover, future work could be performed to compare the effect of HAND1 with other transcription factors (eg, NFIB [nuclear factor I/B], NFIC [nuclear factor I/C], and ZN563 [zinc finger protein 563]) that we explored from motif scan and investigate whether they cooperate with HAND1 in regulating 3D genome organization in DCM.

An intriguing aspect is the possibility of using our discoveries for predicting the risk for developing DCM. A reactivation of HAND1 protein in DCM could indicate the early activation of signaling pathways involved in mesodermal-cardiac differentiation and HAND1 protein induction. In addition, the unique HAND1-mediated H3K27ac looping of genes is likely to play a central role in DCM. This could open novel therapeutic strategies for DCM. For example, signaling pathways blocking HAND1 protein levels (ie, the E3 ligase Fbxo25 [F-box only protein 25] for HAND1⁵⁹) or chemical inhibitors that prevent HAND1 from reprogramming the E-P connectomes leading to DCM could be attractive targets for therapeutic intervention. Our RNA-seq analysis of loop-specific genes uncovered several candidate pathways, such as EZH2 (enhancer of zeste 2 polycomb repressive complex 2 subunit) and TGFβ (transforming growth factor-β), that could be studied further for their therapeutic potential in the hiPSC-CM model.

Limitations

Several limitations to this study exist. First, only 101 donor hearts were used in our study (owing to the availability of *ex vivo* hearts at the Duke Human Heart Repository from Duke University), which may not be representative of all human hearts. Second, although these nonfailing samples were collected from donors without a history of heart failure by Duke Human Heart Repository, noncardiac comorbidities and lifestyle modifications in the nonfailing group may affect the results. Third, because genetic testing is a nonstandard diagnostic workflow in clinical DCM diagnosis, no genetic information on these samples is available, possibly introducing some selection bias for this analysis. Fourth, the heart samples in this study were not age- and sex-matched owing to the limited sample size. The association of these risk factors with 3D chromatin architecture and transcription regulation in DCM requires future study.

Conclusions

On the basis of comprehensive 3D epigenome mapping and functional analysis in human DCM hearts, an induced pluripotent stem cell-derived cardiomyocyte platform, and mouse adult cardiomyocytes, complemented by data from *in vivo* studies of *Hand1*-induced cardiomyocyte hypertrophy and cardiac dilation and dysfunction, our study represents a substantial advance in the understanding of

DCM pathogenesis from a novel view (chromatin topology) and points to HAND1 as a therapeutic target.

ARTICLE INFORMATION

Received May 19, 2021; accepted February 18, 2022.

Affiliations

Botnar Research Centre, Nuffield Department of Orthopaedics, Rheumatology and Musculoskeletal Sciences, University of Oxford, UK (Y.F., F.L., S.P.). Department of Microbiology, Faculty of Medicine, The Chinese University of Hong Kong, China (L.C.). Guangdong Provincial Geriatrics Institute, Guangdong Provincial People's Hospital, Guangdong Academy of Medical Sciences, Guangzhou, China (W. Hong, N.T., Y.M., Q.G., Y.L., L.J.). Institute of Cardiovascular Research, Southwest Medical University, Luzhou, Sichuan, China (C.Z.). College of Engineering and Applied Science (M.W.) and Heart, Lung and Vascular Institute, Department of Internal Medicine, Division of Cardiovascular Health and Disease (M.K., S.S.), University of Cincinnati, OH. Smurfit Institute of Genetics, Trinity College Dublin, Ireland (C.W.). Departments of Pharmacology and Systems Physiology (X.W., J.M., C.G., M.K., G.-C.F.), Pediatrics (A.G.J.), and Pathology and Laboratory Medicine (Y.W., W. Huang), University of Cincinnati College of Medicine, OH. Institute of Cardiovascular Diseases, the First Affiliated Hospital of Guangxi Medical University, Nanning, China (C.L., F.H.). National Clinical Research Center for Geriatrics, West China Hospital, Sichuan University, Chengdu, China (H.C.). Department of Immunology, Weizmann Institute of Science, Rehovot, Israel (S.-Y.W.). Department of Surgery, Cardiovascular & Thoracic, Duke University, Durham, NC (M.J.W.). Division of Biomedical Informatics, Cincinnati Children's Hospital Medical Center, OH (A.G.J.). Department of Computer Science, University of Cincinnati College of Engineering, OH (A.G.J.). Department of OB-GYN/Reproductive, Perinatal and Stem Cell Biology Research, Stanford University, CA (R.A.P.). Departments of Physiology and Cell Biology, the Dorothy M. Davis Heart and Lung Research Institute, Frick Center for Heart Failure and Arrhythmia, the Ohio State University, Columbus (J.-d.F.). Division of Cardiology, Department of Internal Medicine, University of Texas Southwestern Medical Center, Dallas (Z.V.W.).

Acknowledgments

Drs Feng, Pauklin, W. Huang, and Jiang conceptualized and supervised this project and wrote the manuscript. Dr Cai analyzed all the human next-generation sequencing data and wrote the manuscript. Dr C. Wang analyzed the mouse RNA sequencing data. Drs Hong and W. Huang performed the experiments, analyzed data, and wrote the manuscript. Dr X. Wang isolated adult mouse cardiomyocytes. Drs Tan, Y. Wang, Chen, S.-Y. Wang, Liu, F. Huang, Pedersen, Gao, Fan, Sadayappan, and Zhang provided expertise in cardiovascular biology and chromatin biology. Dr M. Wang performed statistical analysis and assisted with interpretation of results. Drs Ma, Kumar, and Fu performed contractility assay, performed calcium transient assay, and interpreted data. Drs Mo and Luo cultured the cells and performed the *in vivo* study. Dr Jegga performed functional enrichment network analysis and provided suggestions for the overall bioinformatics analysis pipeline. M.J.W. provided patient samples and clinical data. Drs Geng and Z.V. Wang provided expertise in cardiovascular biology and chromatin biology. Y. Lin cultured the cells and performed the *in vivo* study.

Sources of Funding

This work was supported by the National Natural Science Foundation of China (grants 81800262 to Dr Jiang, 81670334 to Dr Tan, 81560046 and 81760057 to Dr F. Huang, 81670398 and 91639102 to Dr Zhang, and 31622031, 31671254, and 91749110 to Dr Chen); National Science Foundation of Guangdong Province (grant 2018A030313029 to Dr Jiang); Science and Technology Planning Project of Guangzhou (grant 201903010005 to Dr Jiang); High-level Hospital Construction Project of Guangdong Province (grant DFJH201909 to Tan); National Institutes of Health (grants R01HL160811 and GM-132149 to Dr Fan, R01HL143490, R01HL136025, and R01 HL157456 to Dr Y. Wang, and R01HL139006 to Dr Fu); American Heart Association Career Development Award (grants 20CDA35310176 to W. Huang and 19CDA34630009 to Dr Gao); American Heart Association Postdoctoral Fellowship (grant 834316 to Dr Kumar); Clarendon Fund and St Edmund Hall Scholarship (grant SFF1920_CB_MSD_759707 to Dr Feng); and Cancer Research UK Career Development Fellowship (grant C59392/A25064 to Dr Pauklin). Dr Sadayappan has received support from National Institutes of Health grants R01 AR078001, R01 HL130356, R01 HL105826, R38 HL155775, and R01 HL143490. This work was supported by the American Heart Association 2019 Institutional Undergraduate Student (19UFEL34380251) and Transformation (19TPA34830084) awards, the PLN Foundation (PLN crazy idea), and the Leducq Foundation (Transatlantic Network 18CVD01; PLN-CURE).

Disclosures

Dr Sadayappan participates in consulting and collaborative research studies for the Leducq Foundation (CURE-PLAN [Cure Phospholamban-Induced Cardiomyopathy]), Red Saree Inc, Greater Cincinnati Tamil Sangam, Pfizer, Novo Nordisk, AstraZeneca, MyoKardia, Merck, and Amgen. The other authors report no conflicts.

Supplemental Material

Methods

Figures S1–S8

Tables S1–S4

References 60–87

REFERENCES

- Ziaeian B, Fonarow GC. Epidemiology and aetiology of heart failure. *Nat Rev Cardiol*. 2016;13:368–378. doi: 10.1038/nrcardio.2016.25
- Merlo M, Cannatà A, Gobbo M, Stolfo D, Elliott PM, Sinagra G. Evolving concepts in dilated cardiomyopathy. *Eur J Heart Fail*. 2018;20:228–239. doi: 10.1002/ejhf.1103
- Rosenbaum AN, Agre KE, Pereira NL. Genetics of dilated cardiomyopathy: practical implications for heart failure management. *Nat Rev Cardiol*. 2020;17:286–297. doi: 10.1038/s41569-019-0284-0
- Yu J, Zeng C, Wang Y. Epigenetics in dilated cardiomyopathy. *Curr Opin Cardiol*. 2019;34:260–269. doi: 10.1097/HCO.0000000000000616
- Klemm SL, Shipony Z, Greenleaf WJ. Chromatin accessibility and the regulatory epigenome. *Nat Rev Genet*. 2019;20:207–220. doi: 10.1038/s41576-018-0089-8
- Chatterjee S, Ahituv N. Gene regulatory elements, major drivers of human disease. *Annu Rev Genomics Hum Genet*. 2017;18:45–63. doi: 10.1146/annurev-genom-091416-035537
- Gacita AM, Fullenkamp DE, Ohiri J, Pottinger T, Puckelwartz MJ, Nobrega MA, McNally EM. Genetic variation in enhancers modifies cardiomyopathy gene expression and progression. *Circulation*. 2021;143:1302–1316. doi: 10.1161/CIRCULATIONAHA.120.050432
- Gacita AM, Dellefave-Castillo L, Page PGT, Barefield DY, Wasserstrom JA, Puckelwartz MJ, Nobrega MA, McNally EM. Altered enhancer and promoter usage leads to differential gene expression in the normal and failed human heart. *Circ Heart Fail*. 2020;13:e006926. doi: 10.1161/CIRCHEARTFAILURE.120.006926
- Creyghton MP, Cheng AW, Welstead GG, Kooistra T, Carey BW, Steine EJ, Hanna J, Lodato MA, Frampton GM, Sharp PA, et al. Histone H3K27ac separates active from poised enhancers and predicts developmental state. *Proc Natl Acad Sci U S A*. 2010;107:21931–21936. doi: 10.1073/pnas.1016071107
- Tan WLW, Anene-Nzulu CG, Wong E, Lee CJM, Tan HS, Tang SJ, Perrin A, Wu KX, Zheng W, Ashburn RJ, et al; CHARGE-Heart Failure Working Group, CHARGE-EchoGen Consortium. Epigenomes of human hearts reveal new genetic variants relevant for cardiac disease and phenotype. *Circ Res*. 2020;127:761–777. doi: 10.1161/CIRCRESAHA.120.317254
- Schoenfelder S, Fraser P. Long-range enhancer-promoter contacts in gene expression control. *Nat Rev Genet*. 2019;20:437–455. doi: 10.1038/s41576-019-0128-0
- Mumbach MR, Rubin AJ, Flynn RA, Dai C, Khavari PA, Greenleaf WJ, Chang HY. HiChIP: efficient and sensitive analysis of protein-directed genome architecture. *Nat Methods*. 2016;13:919–922. doi: 10.1038/nmeth.3999
- Mumbach MR, Satpathy AT, Boyle EA, Dai C, Gowen BG, Cho SW, Nguyen ML, Rubin AJ, Granja JM, Kazane KR, et al. Enhancer connectome in primary human cells identifies target genes of disease-associated DNA elements. *Nat Genet*. 2017;49:1602–1612. doi: 10.1038/ng.3963
- Cho SW, Xu J, Sun R, Mumbach MR, Carter AC, Chen YG, Yost KE, Kim J, He J, Nevis SA, et al. Promoter of lncRNA gene PVT1 is a tumor-suppressor DNA boundary element. *Cell*. 2018;173:1398–1412.e22. doi: 10.1016/j.cell.2018.03.068
- Wu S, Turner KM, Nguyen N, Raviram R, Erb M, Santini J, Luebeck J, Rajkumar U, Diao Y, Li B, et al. Circular ecDNA promotes accessible chromatin and high oncogene expression. *Nature*. 2019;575:699–703. doi: 10.1038/s41586-019-1763-5
- Fang R, Yu M, Li G, Chee S, Liu T, Schmitt AD, Ren B. Mapping of long-range chromatin interactions by proximity ligation-assisted ChIP-seq. *Cell Res*. 2016;26:1345–1348. doi: 10.1038/cr.2016.137
- Bertolini JA, Favaro R, Zhu Y, Pagin M, Ngan CY, Wong CH, Tjong H, Vermunt MW, Martynoga B, Barone C, et al. Mapping the global chromatin

connectivity network for Sox2 function in neural stem cell maintenance. *Cell Stem Cell*. 2019;24:462–476.e6. doi: 10.1016/j.stem.2019.02.004

18. Zheng H, Xie W. The role of 3D genome organization in development and cell differentiation. *Nat Rev Mol Cell Biol*. 2019;20:535–550. doi: 10.1038/s41580-019-0132-4
19. Lupiáñez DG, Kraft K, Heinrich V, Krawitz P, Brancati F, Klopocki E, Horn D, Kayserili H, Opitz JM, Laxova R, et al. Disruptions of topological chromatin domains cause pathogenic rewiring of gene-enhancer interactions. *Cell*. 2015;161:1012–1025. doi: 10.1016/j.cell.2015.04.004
20. Flavahan WA, Drier Y, Johnstone SE, Hemming ML, Tarjan DR, Hegazi E, Shareef SJ, Javed NM, Raut CP, Eschle BK, et al. Altered chromosomal topology drives oncogenic programs in SDH-deficient GISTs. *Nature*. 2019;575:229–233. doi: 10.1038/s41586-019-1668-3
21. Poleshko A, Shah PP, Gupta M, Babu A, Morley MP, Manderfield LJ, Ifkovits JL, Calderon D, Aghajanian H, Sierra-Pagán JE, et al. Genome-nuclear lamina interactions regulate cardiac stem cell lineage restriction. *Cell*. 2017;171:573–587.e14. doi: 10.1016/j.cell.2017.09.018
22. Ernst J, Kheradpour P, Mikkelson TS, Shores N, Ward LD, Epstein CB, Zhang X, Wang L, Issner R, Coyne M, et al. Mapping and analysis of chromatin state dynamics in nine human cell types. *Nature*. 2011;473:43–49. doi: 10.1038/nature09906
23. Dirx E, da Costa Martins PA, De Windt LJ. Regulation of fetal gene expression in heart failure. *Biochim Biophys Acta*. 2013;1832:2414–2424. doi: 10.1016/j.bbdis.2013.07.023
24. Chien KR, Knowlton KU, Zhu H, Chien S. Regulation of cardiac gene expression during myocardial growth and hypertrophy: molecular studies of an adaptive physiologic response. *FASEB J*. 1991;5:3037–3046. doi: 10.1096/fasebj.5.15.1835945
25. Heinig M, Adriaens ME, Schafer S, van Deutekom HWM, Lodder EM, Ware JS, Schneider V, Felkin LE, Creemers EE, Meder B, et al. Natural genetic variation of the cardiac transcriptome in non-diseased donors and patients with dilated cardiomyopathy. *Genome Biol*. 2017;18:170. doi: 10.1186/s13059-017-1286-z
26. Celik S, Sadegh MK, Morley M, Roselli C, Ellinor PT, Cappola T, Smith JG, Gidlöf O. Antisense regulation of atrial natriuretic peptide expression. *JCI Insight*. 2019;4:130978. doi: 10.1172/jci.insight.130978
27. Sandhu KS, Li G, Poh HM, Quek YL, Sia YY, Peh SQ, Mulawadi FH, Lim J, Sikic M, Menghi F, et al. Large-scale functional organization of long-range chromatin interaction networks. *Cell Rep*. 2012;2:1207–1219. doi: 10.1016/j.celrep.2012.09.022
28. Huang X, Qu R, Ouyang J, Zhong S, Dai J. An overview of the cytoskeleton-associated role of PDLIM5. *Front Physiol*. 2020;11:975. doi: 10.3389/fphys.2020.00975
29. Wang D, Fang J, Lv J, Pan Z, Yin X, Cheng H, Guo X. Novel polymorphisms in PDLIM3 and PDLIM5 gene encoding Z-line proteins increase risk of idiopathic dilated cardiomyopathy. *J Cell Mol Med*. 2019;23:7054–7062. doi: 10.1111/jcmm.14607
30. Chandra V, Bhattacharyya S, Schmiedel BJ, Madrigal A, Gonzalez-Colin C, Fotsing S, Crinklaw A, Seumois G, Mohammadi P, Kronenberg M, et al. Promoter-interacting expression quantitative trait loci are enriched for functional genetic variants. *Nat Genet*. 2021;53:110–119. doi: 10.1038/s41588-020-00745-3
31. Li G, Ruan X, Auerbach RK, Sandhu KS, Zheng M, Wang P, Poh HM, Goh Y, Lim J, Zhang J, et al. Extensive promoter-centered chromatin interactions provide a topological basis for transcription regulation. *Cell*. 2012;148:84–98. doi: 10.1016/j.cell.2011.12.014
32. Dao LTM, Galindo-Albarrán AO, Castro-Mondragon JA, Andrieu-Soler C, Medina-Rivera A, Souaid C, Charbonnier G, Griffon A, Vanhille L, Stephen T, et al. Genome-wide characterization of mammalian promoters with distal enhancer functions. *Nat Genet*. 2017;49:1073–1081. doi: 10.1038/ng.3884
33. Diao Y, Fang R, Li B, Meng Z, Yu J, Qiu Y, Lin KC, Huang H, Liu T, Marina RJ, et al. A tiling-deletion-based genetic screen for cis-regulatory element identification in mammalian cells. *Nat Methods*. 2017;14:629–635. doi: 10.1038/nmeth.4264
34. Pan YF, Wansa KD, Liu MH, Zhao B, Hong SZ, Tan PY, Lim KS, Bourque G, Liu ET, Cheung E. Regulation of estrogen receptor-mediated long range transcription via evolutionarily conserved distal response elements. *J Biol Chem*. 2008;283:32977–32988. doi: 10.1074/jbc.M802024200
35. Chen J, Bardes EE, Aronow BJ, Jegga AG. ToppGene Suite for gene list enrichment analysis and candidate gene prioritization. *Nucleic Acids Res*. 2009;37:W305–W311. doi: 10.1093/nar/gkp427
36. Steimle JD, Moskowitz IP. TBX5: a key regulator of heart development. *Curr Top Dev Biol*. 2017;122:195–221. doi: 10.1016/bs.ctdb.2016.08.008
37. Yi X, Jiang XJ, Fang ZM. Histone methyltransferase SMYD2: ubiquitous regulator of disease. *Clin Epigenetics*. 2019;11:112. doi: 10.1186/s13148-019-0711-4
38. She P, Zhang H, Peng X, Sun J, Gao B, Zhou Y, Zhu X, Hu X, Lai KS, Wong J, et al. The Gridlock transcriptional repressor impedes vertebrate heart regeneration by restricting expression of lysine methyltransferase. *Development*. 2020;147:dev190678. doi: 10.1242/dev.190678
39. Lu J, McKinsey TA, Zhang CL, Olson EN. Regulation of skeletal myogenesis by association of the MEF2 transcription factor with class II histone deacetylases. *Mol Cell*. 2000;6:233–244. doi: 10.1016/s1097-2765(00)00025-3
40. Kim Y, Phan D, van Rooij E, Wang DZ, McAnally J, Qi X, Richardson JA, Hill JA, Bassel-Duby R, Olson EN. The MEF2D transcription factor mediates stress-dependent cardiac remodeling in mice. *J Clin Invest*. 2008;118:124–132. doi: 10.1172/JCI33255
41. Bang ML, Mudry RE, McElhinny AS, Trombitás K, Geach AJ, Yamasaki R, Sorimachi H, Granzier H, Gregorio CC, Labeit S. Myopalladin, a novel 145-kilodalton sarcomeric protein with multiple roles in Z-disc and I-band protein assemblies. *J Cell Biol*. 2001;153:413–427. doi: 10.1083/jcb.153.2.413
42. Ramaccini D, Montoya-Urbe V, Aan FJ, Modesti L, Potes Y, Wieckowski MR, Krga I, Glibetić M, Pinton P, Giorgi C, et al. Mitochondrial function and dysfunction in dilated cardiomyopathy. *Front Cell Dev Biol*. 2020;8:624216. doi: 10.3389/fcell.2020.624216
43. Andersson C, Lin H, Liu C, Levy D, Mitchell GF, Larson MG, Vasan RS. Integrated multiomics approach to identify genetic underpinnings of heart failure and its echocardiographic precursors: Framingham Heart Study. *Circ Genom Precis Med*. 2019;12:e002489. doi: 10.1161/CIRCGEN.118.002489
44. Yasuda-Yamahara M, Rogg M, Yamahara K, Maier JI, Huber TB, Schell C. AIF1L regulates actomyosin contractility and filopodial extensions in human podocytes. *PLoS One*. 2018;13:e0200487. doi: 10.1371/journal.pone.0200487
45. Brody MJ, Hacker TA, Patel JR, Feng L, Sadoshima J, Tevosian SG, Balijepalli RC, Moss RL, Lee Y. Ablation of the cardiac-specific gene leucine-rich repeat containing 10 (Lrrc10) results in dilated cardiomyopathy. *PLoS One*. 2012;7:e51621. doi: 10.1371/journal.pone.0051621
46. Buenostro JD, Giresi PG, Zaba LC, Chang HY, Greenleaf WJ. Transposition of native chromatin for fast and sensitive epigenomic profiling of open chromatin, DNA-binding proteins and nucleosome position. *Nat Methods*. 2013;10:1213–1218. doi: 10.1038/nmeth.2688
47. Dixon JR, Gorkin DU, Ren B. Chromatin domains: the unit of chromosome organization. *Mol Cell*. 2016;62:668–680. doi: 10.1016/j.molcel.2016.05.018
48. Nora EP, Lajoie BR, Schulz EG, Giorgetti L, Okamoto I, Servant N, Piolot T, van Berkum NL, Meisig J, Sedat J, et al. Spatial partitioning of the regulatory landscape of the X-inactivation centre. *Nature*. 2012;485:381–385. doi: 10.1038/nature11049
49. Xu J, Gong NL, Bodi I, Aronow BJ, Backx PH, Molkentin JD. Myocyte enhancer factors 2A and 2C induce dilated cardiomyopathy in transgenic mice. *J Biol Chem*. 2006;281:9152–9162. doi: 10.1074/jbc.M510217200
50. Riley P, Anson-Cartwright L, Cross JC. The Hand1 bHLH transcription factor is essential for placentation and cardiac morphogenesis. *Nat Genet*. 1998;18:271–275. doi: 10.1038/ng0398-271
51. Zhou YM, Dai XY, Qiu XB, Yuan F, Li RG, Xu YJ, Qu XK, Huang RT, Xue S, Yang YQ. HAND1 loss-of-function mutation associated with familial dilated cardiomyopathy. *Clin Chem Lab Med*. 2016;54:1161–1167. doi: 10.1515/ccim-2015-0766
52. Sun N, Yazawa M, Liu J, Han L, Sanchez-Freire V, Abilez OJ, Navarrete EG, Hu S, Wang L, Lee A, et al. Patient-specific induced pluripotent stem cells as a model for familial dilated cardiomyopathy. *Sci Transl Med*. 2012;4:130ra47. doi: 10.1126/scitranslmed.3003552
53. Knight WE, Chen S, Zhang Y, Oikawa M, Wu M, Zhou Q, Miller CL, Cai Y, Mickelsen DM, Moravec C, et al. PDE1C deficiency antagonizes pathological cardiac remodeling and dysfunction. *Proc Natl Acad Sci U S A*. 2016;113:E7116–E7125. doi: 10.1073/pnas.1607728113
54. Mørk HK, Sjaastad I, Sande JB, Periasamy M, Sejersted OM, Louch WE. Increased cardiomyocyte function and Ca²⁺ transients in mice during early congestive heart failure. *J Mol Cell Cardiol*. 2007;43:177–186. doi: 10.1016/j.yjmcc.2007.05.004
55. Mørk HK, Sjaastad I, Sejersted OM, Louch WE. Slowing of cardiomyocyte Ca²⁺ release and contraction during heart failure progression in postinfarction mice. *Am J Physiol Heart Circ Physiol*. 2009;296:H1069–H1079. doi: 10.1152/ajpheart.01009.2008
56. Zhao SM, Wang YL, Guo CY, Chen JL, Wu YQ. Progressive decay of Ca²⁺ homeostasis in the development of diabetic cardiomyopathy. *Cardiovasc Diabetol*. 2014;13:75. doi: 10.1186/1475-2840-13-75

57. Liu X, Zhang Y, Chen Y, Li M, Zhou F, Li K, Cao H, Ni M, Liu Y, Gu Z, et al. In situ capture of chromatin interactions by biotinylated dCas9. *Cell*. 2017;170:1028–1043.e19. doi: 10.1016/j.cell.2017.08.003
58. Misteli T. The self-organizing genome: principles of genome architecture and function. *Cell*. 2020;183:28–45. doi: 10.1016/j.cell.2020.09.014
59. Jang JW, Lee WY, Lee JH, Moon SH, Kim CH, Chung HM. A novel Fbxo25 acts as an E3 ligase for destructing cardiac specific transcription factors. *Biochem Biophys Res Commun*. 2011;410:183–188. doi: 10.1016/j.bbrc.2011.05.011
60. Ewels P, Magnusson M, Lundin S, Käller M. MultiQC: summarize analysis results for multiple tools and samples in a single report. *Bioinformatics*. 2016;32:3047–3048. doi: 10.1093/bioinformatics/btw354
61. Li H, Durbin R. Fast and accurate short read alignment with Burrows-Wheeler transform. *Bioinformatics*. 2009;25:1754–1760. doi: 10.1093/bioinformatics/btp324
62. Feng J, Liu T, Qin B, Zhang Y, Liu XS. Identifying ChIP-seq enrichment using MACS. *Nat Protoc*. 2012;7:1728–1740. doi: 10.1038/nprot.2012.101
63. Robinson MD, McCarthy DJ, Smyth GK. edgeR: a Bioconductor package for differential expression analysis of digital gene expression data. *Bioinformatics*. 2010;26:139–140. doi: 10.1093/bioinformatics/btp616
64. Dobin A, Davis CA, Schlesinger F, Drenkow J, Zaleski C, Jha S, Batut P, Chaisson M, Gingeras TR. STAR: ultrafast universal RNA-seq aligner. *Bioinformatics*. 2013;29:15–21. doi: 10.1093/bioinformatics/bts635
65. Li H, Handsaker B, Wysoker A, Fennell T, Ruan J, Homer N, Marth G, Abecasis G, Durbin R; 1000 Genome Project Data Processing Subgroup. The Sequence alignment/map format and SAMtools. *Bioinformatics*. 2009;25:2078–2079. doi: 10.1093/bioinformatics/btp352
66. Liao Y, Smyth GK, Shi W. featureCounts: an efficient general purpose program for assigning sequence reads to genomic features. *Bioinformatics*. 2014;30:923–930. doi: 10.1093/bioinformatics/btt656
67. Love MI, Huber W, Anders S. Moderated estimation of fold change and dispersion for RNA-seq data with DESeq2. *Genome Biol*. 2014;15:550. doi: 10.1186/s13059-014-0550-8
68. Servant N, Varoquaux N, Lajoie BR, Viara E, Chen CJ, Vert JP, Heard E, Dekker J, Barillot E. HiC-Pro: an optimized and flexible pipeline for Hi-C data processing. *Genome Biol*. 2015;16:259. doi: 10.1186/s13059-015-0831-x
69. Durand NC, Shamim MS, Machol I, Rao SS, Huntley MH, Lander ES, Aiden EL. Juicer provides a one-click system for analyzing loop-resolution Hi-C experiments. *Cell Syst*. 2016;3:95–98. doi: 10.1016/j.cels.2016.07.002
70. Ramírez F, Dündar F, Diehl S, Grüning BA, Manke T. deepTools: a flexible platform for exploring deep-sequencing data. *Nucleic Acids Res*. 2014;42:W187–W191. doi: 10.1093/nar/gku365
71. Phanstiel DH, Boyle AP, Heidari N, Snyder MP. Mango: a bias-correcting ChIA-PET analysis pipeline. *Bioinformatics*. 2015;31:3092–3098. doi: 10.1093/bioinformatics/btv336
72. Li G, Sun T, Chang H, Cai L, Hong P, Zhou Q. Chromatin interaction analysis with updated ChIA-PET tool (V3). *Genes*. 2019;10:554–581. doi: 10.3390/genes10070554
73. Naumova N, Smith EM, Zhan Y, Dekker J. Analysis of long-range chromatin interactions using chromosome conformation capture. *Methods*. 2012;58:192–203. doi: 10.1016/j.jymeth.2012.07.022
74. Hagège H, Klous P, Braem C, Splinter E, Dekker J, Cathala G, de Laat W, Forné T. Quantitative analysis of chromosome conformation capture assays (3C-qPCR). *Nat Protoc*. 2007;2:1722–1733. doi: 10.1038/nprot.2007.243
75. Shannon P, Markiel A, Ozier O, Baliga NS, Wang JT, Ramage D, Amin N, Schwikowski B, Ideker T. Cytoscape: a software environment for integrated models of biomolecular interaction networks. *Genome Res*. 2003;13:2498–2504. doi: 10.1101/gr.1239303
76. Abdennur N, Mirny LA. Cooler: scalable storage for Hi-C data and other genomically labeled arrays. *Bioinformatics*. 2020;36:311–316. doi: 10.1093/bioinformatics/btz540
77. Crane E, Bian Q, McCord RP, Lajoie BR, Wheeler BS, Ralston EJ, Uzawa S, Dekker J, Meyer BJ. Condensin-driven remodelling of X chromosome topology during dosage compensation. *Nature*. 2015;523:240–244. doi: 10.1038/nature14450
78. Wolff J, Rabbani L, Gilsbach R, Richard G, Manke T, Backofen R, Grüning BA. Galaxy HiCExplorer 3: a web server for reproducible Hi-C, capture Hi-C and single-cell Hi-C data analysis, quality control and visualization. *Nucleic Acids Res*. 2020;48:W177–W184. doi: 10.1093/nar/gkaa220
79. Gong Y, Lazaris C, Sakellaropoulos T, Lozano A, Kambadur P, Ntziachristos P, Aifantis I, Tsirigos A. Stratification of TAD boundaries reveals preferential insulation of super-enhancers by strong boundaries. *Nat Commun*. 2018;9:542. doi: 10.1038/s41467-018-03017-1
80. Quinlan AR, Hall IM. BEDTools: a flexible suite of utilities for comparing genomic features. *Bioinformatics*. 2010;26:841–842. doi: 10.1093/bioinformatics/btq033
81. Yang T, Zhang F, Yardımcı GG, Song F, Hardison RC, Noble WS, Yue F, Li Q. HiCRep: assessing the reproducibility of Hi-C data using a stratum-adjusted correlation coefficient. *Genome Res*. 2017;27:1939–1949. doi: 10.1101/gr.220640.117
82. Thorvaldsdóttir H, Robinson JT, Mesirov JP. Integrative Genomics Viewer (IGV): high-performance genomics data visualization and exploration. *Brief Bioinform*. 2013;14:178–192. doi: 10.1093/bib/bbs017
83. Carroll KJ, Makarewich CA, McAnally J, Anderson DM, Zentili L, Liu N, Giacca M, Bassel-Duby R, Olson EN. A mouse model for adult cardiac-specific gene deletion with CRISPR/Cas9. *Proc Natl Acad Sci U S A*. 2016;113:338–343. doi: 10.1073/pnas.1523918113
84. Huang W, Feng Y, Liang J, Yu H, Wang C, Wang B, Wang M, Jiang L, Meng W, Cai W, et al. Loss of microRNA-128 promotes cardiomyocyte proliferation and heart regeneration. *Nat Commun*. 2018;9:700. doi: 10.1038/s41467-018-03019-z
85. Kumar M, Haghighi K, Kranias EG, Sadayappan S. Phosphorylation of cardiac myosin-binding protein-C contributes to calcium homeostasis. *J Biol Chem*. 2020;295:11275–11291. doi: 10.1074/jbc.RA120.013296
86. Dai B, Huang W, Xu M, Millard RW, Gao MH, Hammond HK, Menick DR, Ashraf M, Wang Y. Reduced collagen deposition in infarcted myocardium facilitates induced pluripotent stem cell engraftment and angiomyogenesis for improvement of left ventricular function. *J Am Coll Cardiol*. 2011;58:2118–2127. doi: 10.1016/j.jacc.2011.06.062
87. Ma J, Hong K, Wang HS. Progesterone protects against bisphenol a-induced arrhythmias in female rat cardiac myocytes via rapid signaling. *Endocrinology*. 2017;158:778–790. doi: 10.1210/en.2016-1702